ACS Biomaterials SCIENCE & ENGINEERING

pubs.acs.org/journal/abseba

Article

Does the Extracellular Matrix Support Cell–Cell Communication by Elastic Wave Packets?

Artem Y. Panchenko,[#] Oren Tchaicheeyan,[#] Igor E. Berinskii,[*] and Ayelet Lesman[*]

Cite This: *ACS Biomater. Sci. Eng.* 2022, 8, 5155–5170

Read Online

ACCESS | Metrics & More | Article Recommendations | Supporting Information

ABSTRACT: The extracellular matrix (ECM) is a fibrous network supporting biological cells and provides them a medium for interaction. Cells modify the ECM by applying traction forces, and these forces can propagate to long ranges and establish a mechanism of mechanical communication between neighboring cells. Previous studies have mainly focused on analysis of static force transmission across the ECM. In this study, we explore the plausibility of dynamic mechanical interaction, expressed as vibrations or abrupt fluctuations, giving rise to elastic waves propagating along ECM fibers. We use a numerical mass-spring model to simulate the longitudinal and transversal waves propagating along a single ECM fiber and across a 2D random fiber network. The elastic waves are induced by an active contracting cell (signaler) and received by a passive neighboring cell (receiver). We show that dynamic wave propagation may amplify the signal at the receiver end and support up to an order of magnitude stronger mechanical cues and longer-ranged communication relative to static transmission. Also, we report an optimal impulse duration corresponding to the most effective transmission, as well as extreme fast impulses, in which the waves are encaged around the active cell and do not reach the neighboring cell, possibly due to the Anderson localization effect. Finally, we also demonstrate that extracellular fluid viscosity reduces, but still allows, dynamic propagation along embedded ECM fibers. Our results motivate future biological experiments in mechanobiology to investigate, on the one hand, the mechanosensitivity of cells to dynamic forces traveling and guided by the ECM and, on the other hand, the impact of ECM architecture and remodeling on dynamic force transmission and its spectral filtering, dispersion, and decay.

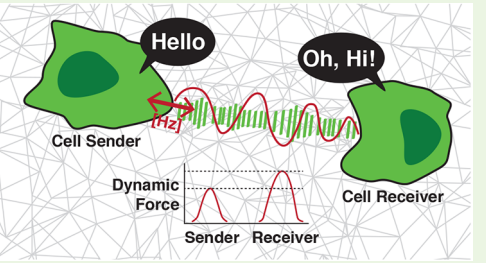

KEYWORDS: *mechanobiology, extracellular matrix, cell-ECM interaction, dynamic communication, random elastic network, fibrous networks, hydrogel*

INTRODUCTION

The field of cell–extracellular matrix (ECM) mechanical interaction has grown tremendously since the 1980s.[1−3] One of the foremost observations is that ECM nonlinear visco-elasto-plastic mechanical properties can have a direct effect on cell fate. Reciprocally, cells modify the ECM by applying traction forces and these forces can propagate to long ranges and with unique patterns of force chains across the ECM.[4,5] Indeed, when seeded in fibrous biological hydrogels, cells modify the ECM from initially isotropic state to more axially or radially aligned,[6,7] generating what are commonly referred to as ECM bridges, bundles, bands, or tethers.[7−9] These ECM regions of highly directional alignment and tension can couple, over long ranges (∼10 cell sizes) and with strong directionality, living cells, and mediate their mechanical communication.[4,10−24]

Whereas the focus has been on ECM-mediated and effectively transmitted static mechanical forces, we would like to explore in this study the plausibility of dynamic mechanical interaction between cells through the ECM. By "dynamic," we mean exchange of fast traveling elastic wave packets. This dynamic effect may be expressed in many forms such as vibrations, cyclic fluctuations, ECM fiber yanking or tugging (due to jerking or snapping), pulsatile rhythmic undulations, bursts of quasi-periodic force oscillations, and cytoquakes (anomalously large, sudden motions—avalanches—of the cytoskeleton),[25,26] propagating waves or quick-release perturbations. We propose that dynamic mechanical interaction is relatively efficient and support our hypothesis with numerical simulations.

By definition, communication is a process between a signaler and a receiver in which information in the form of temporally modulated energy is transmitted between the two sides.[27] At the level of whole organisms, vibration and chemicals are assumed to be the oldest modes of communication and both probably evolved from the original cell–cell mechanical and chemical interactions within early metazoans.[28] Even small

Received: September 4, 2022
Accepted: October 24, 2022
Published: November 8, 2022

https://doi.org/10.1021/acsbiomaterials.2c01049
ACS Biomater. Sci. Eng. 2022, 8, 5155–5170

microorganisms vibrate in response to their metabolic activity and nanoscale vibrations is a signature of life.[29] Biotremology is a recently emergent field of study of vibratory communication behavior through use of substrate-borne, boundary or surface, and mechanical waves.[30] Such mechanocommunication modality was demonstrated in creatures as big as elephants and as small as spiders.[31−34] Recently, this communication modality has been implemented into robotics.[35] Our study explores the ability of the fibrous ECM to effectively deliver dynamic forces between contractile cells, as a potential mechanism of vibrational communication. Indeed, ECM vibroscape (i.e., vibrational "landscape") may be crucial for such mechanocommunication efficiency. Whereas static force exertion (i.e., constant force applied for a time scale much larger than the time required for a traveling elastic wave to completely decay) is expected to be metabolically costly and induce long-term desensitization at the receiver end, dynamic forces (driven fluctuations) are expected to allow for metabolically efficient interaction and higher information content, filter noise and reduce noise by cycle integration,[14] and allow for faster signal transmission and longer range transmission.[36,37]

Single cells, using their actomyosin machinery, may pluck,[38] tug,[39] twitch, or abruptly release tensed ECM fibers.[40] The following plausible mechanisms may be involved in causing elastic wave packet traveling in the ECM: (i) cytoskeletal machinery oscillations of the actomyosin stress fibers, sarcomeres, or the cortex.[41] Whereas cardiomyocytes synchronously beat at ∼1 Hz, arrhythmic cardiomyocytes can beat at "bursting behavior" up to few Hz.[15] Also, myocytes may vibrate at 10s up 100s of Hz,[42] and ciliated cells in ear and gut oscillate at few 10s of Hz;[43] (ii) cell membrane fluctuations, such as local sub-micron mechanical out-of-plane oscillations of the cell surface.[44,45] Cell membrane nm fluctuations are in the 1 kHz range, coined "flickering."[46] Lymphocytes and monocytes display 20−30 nm undulations at up to 30 Hz;[45,47] (iii) quick focal adhesion detachment or disassembly. High frequency fluctuations can appear when a cell pulls on the ECM and then abruptly releases the built-up tension, for example, as a cell migrates, the exerted forces on the ECM fibers may cause vibrations to the surroundings.[40,48−50] Interestingly, myosin motor attachment and detachment rates are in the order of 35 Hz and 350 Hz, respectively; and (iv) tensegrity vibrations are high frequency natural modes arising due to cytoskeletal tension.[51−53]

Apart from their ability to exert dynamic forces, cells are mechanosensitive[54] to dynamic stimuli and have shown to demonstrate (i) modified cytoskeletal structure and its fluidization at high stretch rates;[55,56] (ii) mechanoptosis;[57] (iii) mechanotropism;[58] (iv) altered ECM expression and remodeling;[59−65] (v) increase culture cell growth rate by nanokicking;[47,66,67] (vi) torsional and translational vibrations of the cell nucleus;[53] (vii) synchronization of beating cardiomyocytes,[10,15] (viii) higher cellular viability at specific frequency and amplitude ranges,[68] and (ix) altered collective cell migration.[69]

As for the substrate that carries these perturbations, the prestressed ECM fibers,[40,70,71] being a constituent of a hydrogel with both storage and loss moduli, are expected to more significantly overdamp transverse waves and mainly allow underdamped longitudinal stretch waves.[21,72] Traveling longitudinal waves transfer momentum and energy, and therefore, as the wave reaches the neighboring cell, the local mechanical impedance mismatch will rebound the imparted wave and the cell is expected to experience a pushback, while sensing either increased forces and/or displacements. Moreover, the ECM is filled with an extracellular fluid (ECF) in between the ECM fibers, and the viscosity of the ECF may overdamp wave propagation along ECM fibers. Yet, it is still not fully understood how perturbations propagate along ECM fibers as part of cell−cell mechanical interaction and the influence of ECF viscosity and structure on such interaction.

We examined in this work, by numerical modeling and simulations, the impact of traveling elastic waves, both transverse and longitudinal, sent by an actively contracting cell (signaler) and received by a passive neighboring cell (receiver). For the receiver end, two extreme displacement boundary conditions were studied, either fixed (zero displacement) or free (unconstrained). We show that for dynamic interaction, tension (in the case of "fixed end") and displacement (in the case of "free-end") are greater at the receiver end and up to an order of magnitude stronger relative to static interaction, thus supporting stronger mechanical cue and longer-ranged communication. The range of mechanical influence may extend by an order of magnitude when forces propagate dynamically through the ECM fibers rather than statically. We observe that ECF viscosity indeed reduces the dynamic effect through the action of viscous drag leading to dissipation of transverse-wave elastic energy; however, fast-spreading longitudinal-wave elastic energy may still cause a considerable increase in forces acting on the *passive* cell.

Our findings are relevant to the field of ECM-mediated cell−cell mechanical communication, cell migration, cell morphodynamics, cell-to-cell mechanical synchronization, mechanotropism, and design of active biomaterials for mechanobiology.[73−82] Finally, our theoretical work provides motivation for future biological experiments in mechanobiology to investigate, on the one hand, the mechanosensitivity of cells to dynamic forces traveling and guided by the ECM and, on the other hand, the impact of ECM architecture and remodeling on transmitted ECM waves.

METHODS

Fiber Simulations. Single-fiber dynamics is studied analytically and using a discrete computational model. The analytical solution for the case of a single fiber is considered in detail in the Materials and Methods section in the Supporting Information. We employ discrete fiber simulations to study the response of a single fiber and 2D fiber networks to cell contraction and the mechanical signal reaching a neighboring cell. Each fiber is represented as a set of nodes with point masses connected by links moving in the 2D space due to the linear interaction with neighboring connected nodes, action of the external forces, and initial and boundary conditions. Hereinafter, we refer to vectors in bold and scalars in nonbold italic symbols.

Let us consider a specific link of the network with the index k. The link is characterized by the vector $\boldsymbol{d}_k$ connecting two adjacent nodes. Scalar values d_k and a_k correspond to the actual and equilibrium lengths of the link correspondingly. The energy of a specific link is described by a harmonic potential

$$U_k = \frac{EA}{2a_k}(d_k - a_k)^2 \tag{1}$$

where E is Young's modulus, A is a fiber section area, and $\frac{EA}{a_k}$ is an axial stiffness of the fiber. So, force between two nodes is

$$\boldsymbol{F}_k = -\frac{\partial U}{\partial \boldsymbol{d}_k} = -EA(d_k - a_k)\frac{\boldsymbol{d}_k}{d_k a_k} = EA\left(\frac{1}{a_k} - \frac{1}{d_k}\right)\boldsymbol{d}_k \tag{2}$$

https://doi.org/10.1021/acsbiomaterials.2c01049
ACS Biomater. Sci. Eng. 2022, 8, 5155−5170

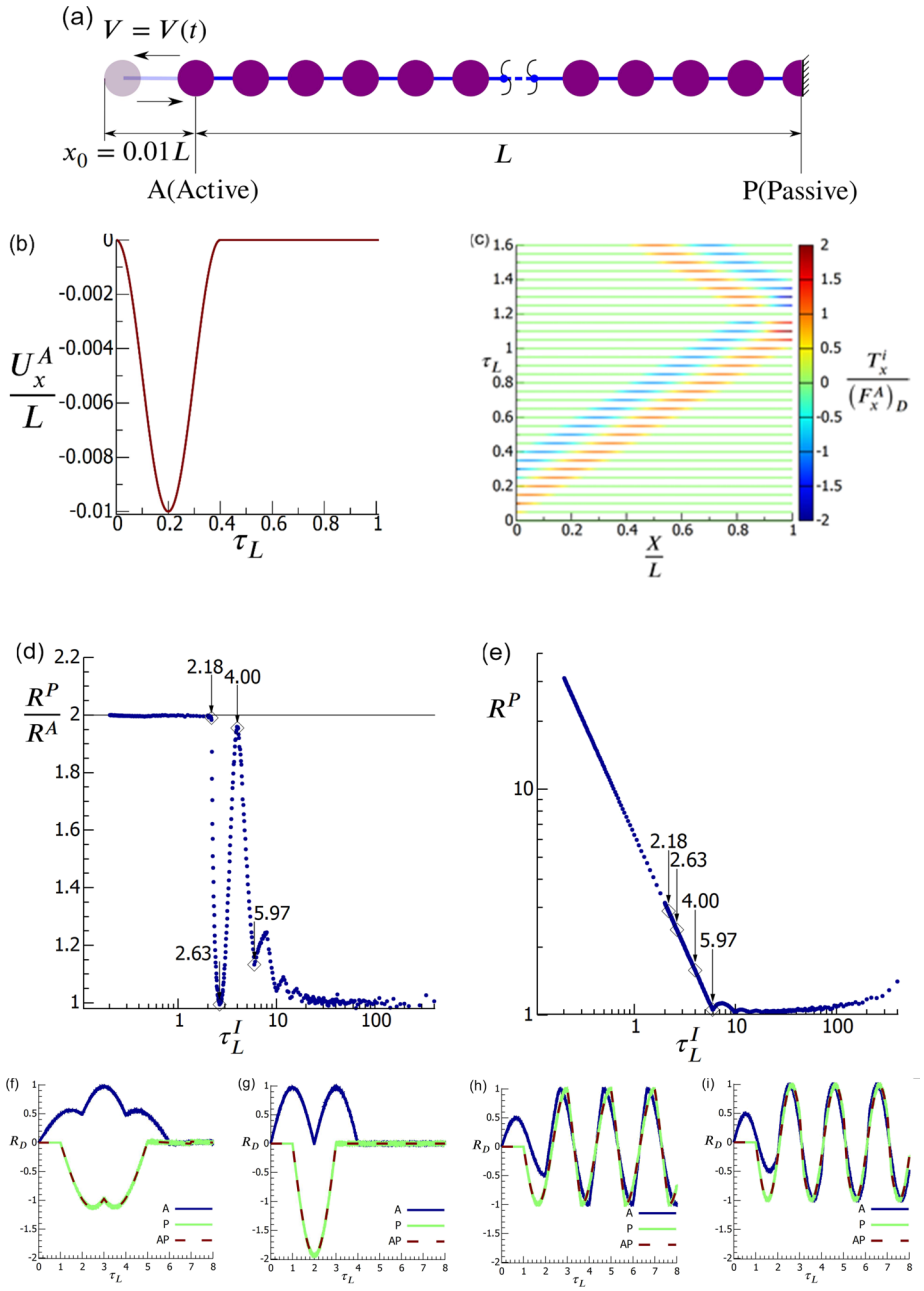

Figure 1. Longitudinal wave propagation along a single fiber. (a) Schematics of the single-fiber model. The wave is a result of a pull−push longitudinal displacement perturbation (U_x^A) applied on a single linear elastic fiber of length L, at its "*active*" end, with an amplitude of 1% of total fiber length (L). (b) Displacement along X of the *active* node as a function of the normalized time $\tau_L = \frac{t}{t_L}$, with t_L being the time needed for the perturbed wave to reach the end of the fiber. (c) Tension distribution in the chain along X and its time evolution. The color bar depicts the ratio of fiber tension, T_x^i, over time, relative to the maximal tension at the *active* end during a dynamic perturbation, $(F_x^A)_D$; red color denotes tension, blue color denotes compression, and green denotes an elastically relaxed fiber; (d) ratio of maximum force on *passive* node to maximum force on *active* node; (e) R^P, ratio of maximum force on *passive* node to the static force; the perturbation is applied at different perturbation normalized impulse times $\tau_L^I = \frac{t_I}{t_L}$, with t_I being the impulse time. (f−i) Force acting at the *active* end (A, blue line), *passive* end (P, green line), and analytically calculated *passive* end (AP, red dashed line) normalized by the maximum force at the *active* end, as a function of dimensionless time (τ_L) for specific impulse periods: τ_L^I = 5.97 (f); 4.00 (g); 2.63 (h), and 2.18 (i).

The motion of a single node in the string or 2D network can be described by the equation

$$\ddot{\boldsymbol{r}}_i = \frac{1}{m_i}\sum_k (\boldsymbol{F}_{k,i} - \boldsymbol{T}_{k,i}) \tag{3}$$

Here, $\boldsymbol{r}_i$ is a position vector of the node i, $\boldsymbol{F}_{k,i}$ is a force acting on a i-th node from the adjacent link k, and $\boldsymbol{T}_{k,i}$ is a drag force due to surrounding fluid viscosity (presented in the next paragraph). Mass of i-th node m_i is defined as

$$m_i = \sum_k \lambda \frac{a_k}{2} \tag{4}$$

where k passes over all links connected to the considered node and λ is the linear fiber density. Numerical integration of eq 3 for each node

https://doi.org/10.1021/acsbiomaterials.2c01049
ACS Biomater. Sci. Eng. 2022, 8, 5155−5170

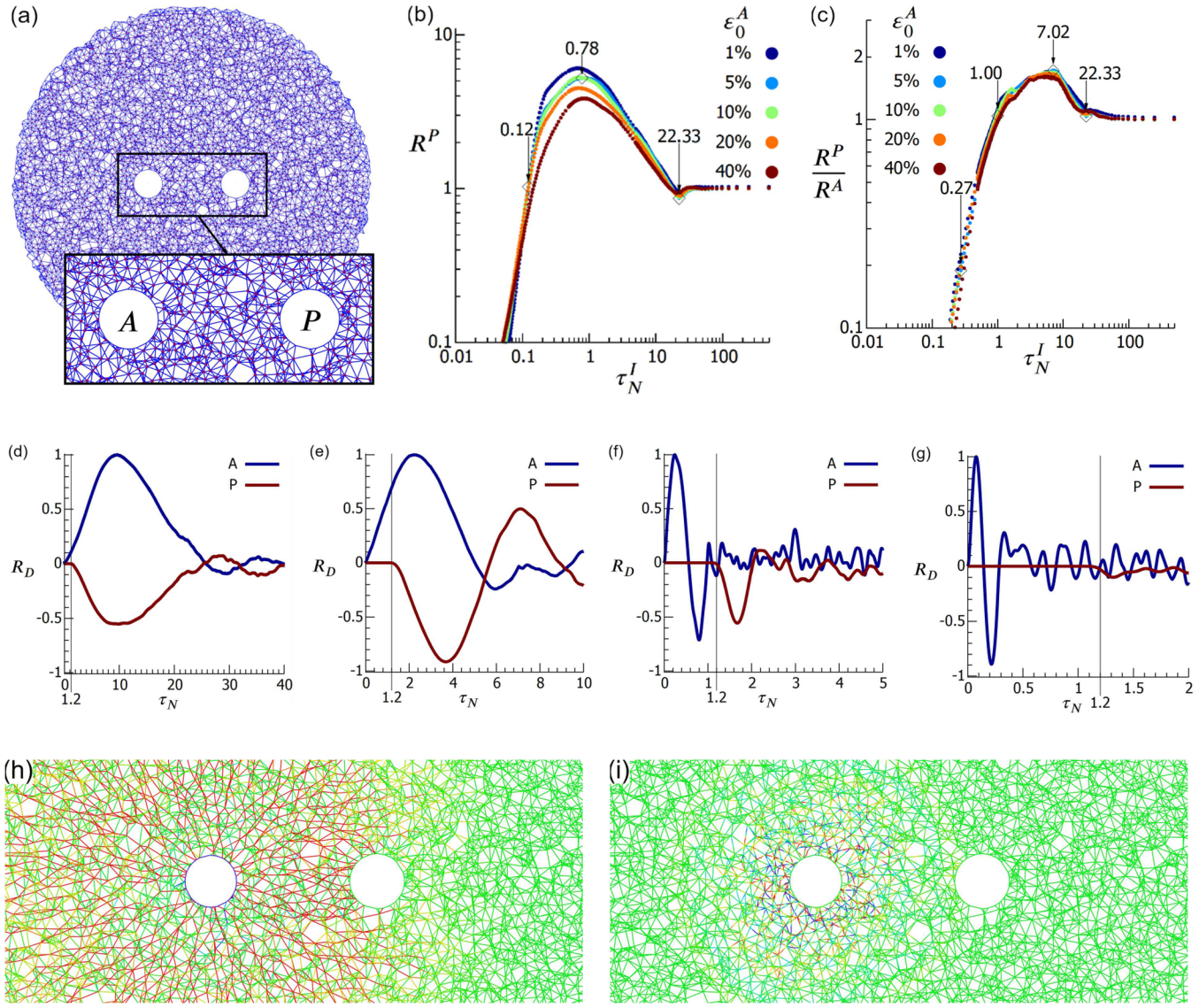

Figure 2. Wave propagation across a 2D fibrous network induced by an active contractile cell toward a neighboring *passive* cell. Distance between cells is $d = 6R_0$ (cell radii). (a) Two cells embedded within a 2D fibrous network, with an *active* cell (A) and a *passive* cell (P). (b) Dynamic-to-static ratio of the maximum force on the *passive* cell (on the side that faces the *active* cell) to the corresponding force in the static case. (c) Ratio of *passive-to-active* forces, quantifying the ratio of the maximum force on the *passive* cell to maximum force on the *active* cell (on the sides facing each other). (d–g) Force over time (normalized time, defined as $\tau_N = \frac{t}{t_N}$) on the *active* cell (blue) and on the *passive* cell (red), for several perturbation periods τ_N^I= 22.33 (*d*), 7.02 (*e*), 1.00 (*f*), and 0.27 (*g*). (h,i) Snapshot images showing force (F_x) distribution along network fibers at the time corresponding to the maximum force acting on the *passive* cell for τ_N^I = 7.02 (h) and 0.27 (i). Force F_x is normalized by the *maximal* force that appeared on the *active* cell, $(F_x^A)_D$. See corresponding Movies S1 and S2.

is carried out using the leapfrog integrator[83] with a chosen time step of $\Delta\tau = 5 \times 10^{-4}\tau_*$. Here

$$\tau_* = \min\left(\pi \cdot \sqrt{\frac{m_i}{\frac{EA}{a_k}}}\right)\Big|_{\forall\{i,k\}} = \frac{\pi}{\sqrt{EA}}\min\left(\sqrt{m_i \cdot a_k}\right)\Big|_{\forall\{i,k\}} \tag{5}$$

where the index i passes over all nodes in the network and k passes over the links adjacent to node i.

Viscosity Model. Accounting for the effect of fluid surrounding the fibers was carried out using the approach proposed in a previous computational study.[84] For simplification, we assume that the fluid is stationary. We consider the fiber element k as a cylinder and its movements along the axis (defined by the unit vector $\boldsymbol{e}_{1,k}$) and orthogonal to it (unit vector $\boldsymbol{e}_{2,k}$). In this case, the components of the drag force acting on the element of an infinite cylinder can be found from the equations[84]

$$dT_{1,k} = A_1 \upsilon_1 dl \tag{6.1}$$

$$dT_{2,k} = A_2 \upsilon_2 dl \tag{6.2}$$

$$A_1 = \frac{2\pi r^f \mu}{r^t \ln\left(\frac{r^t}{r^f}\right)} \quad A_2 = \frac{4\pi\mu}{\ln\left(\frac{7.4}{Re}\right)} \tag{6.3}$$

where μ (constant) is the dynamic ECF viscosity; r^f is fiber radius (constant); υ_1, υ_2 are the components of the link velocity vector; dl is a link length; $Re = \frac{2\upsilon r^f \rho}{\mu}$ is Reynolds number; $\upsilon = \sqrt{\upsilon_1^2 + \upsilon_2^2}$ is a link speed; r^t is an average distance between the fibers determined by their concentration for each network; and ρ is a fluid density. Thus, the

https://doi.org/10.1021/acsbiomaterials.2c01049
ACS Biomater. Sci. Eng. 2022, 8, 5155−5170

element is affected by a force and a moment defined as an integral over dT_1 and dT_2. For additional details of the integration, see ref 84 and eqs S7−S14. The parameters used for the calculations are given in Table S2.

Calculations were performed by in-house C++ code combined with Compute United Device Architecture (CUDA) to increase its performance.[85] At every time step, all forces acting on a single node from the neighbor nodes are computed using the right part of eqs 2 and 6.1 by a single GPU thread. Then, the thread integrates eq 3 to obtain the velocities and displacements of each node. The code used for the simulation is available at https://github.com/MSMS-LAB/END-SYM.

Single Fiber. For the simulations of a single-fiber dynamics with longitudinal waves, we used the mass-spring model shown in Figure 1a. The simulations were performed with 3000 equally spaced nodes. As the considered problem is linear, it does not depend on the specific parameters of stiffness, mass, and initial link length. The case of transverse waves is considered in the Materials and Methods section in the Supporting Information.

At the initial moment, a velocity function is assigned to the left-most particle (*active*-end)

$$v(t) = \begin{cases} -\frac{\pi}{2} v_0 \sin \frac{\pi\, t\, v_0}{x_0}, \; 0 < t < 2\frac{x_0}{v_0} \\ 0, \; t > 2\frac{x_0}{v_0} \end{cases} \tag{7}$$

Here, x_0 is the displacement amplitude, $v_0 = 2\frac{x_0}{t_I}$ is the average speed; and t_I is the impulse duration. The velocity of the *active* node is set either in longitudinal (Figure 1a) or transverse (Figure S1a) direction. The corresponding equations of motion are solved numerically according to the method explained above. To ensure smoothness of force build-up, the temporal derivatives of displacement perturbation (i.e., the perturbation velocity) at the start and finish were set to zero.

Random Fiber Network. We use MATLAB (R2020b, Natick, MA, Copyright 1984−2018 The MathWorks, Inc.) to create the fiber network geometry and architecture, as we previously described.[4] The MATLAB codes are available at request (A.L.). We designed the 2D mass-spring networks to have an isotropic distribution of fiber orientations, a homogeneous density, and a controlled connectivity (coordination number).[86,87] Finally, a single cell or two cells are embedded in the network by removing fibers and nodes in circular domains in the center of the network (Figure 2a). The circular geometry of the modeled cells may represent contractile cells that are relatively spherical, such as during the early stage of cells interacting with biopolymer gels[88] or cells that are inherently more rounded when embedded in gels like some types of cancer or epithelial cells.[89]

The size of the network is 25 times larger than the cell radius, in which case the decay of displacements in the simulated network near the cell is not sensitive to the specific boundary conditions set at the outer boundary. We, therefore, choose to fix the displacements to be zero at the outer boundary of the network. Two cells are distanced 6 radii apart unless mentioned otherwise.

To model cell contraction in fibrous networks, we consider two cells, an *active* one (A) and a *passive* one (P). The *active* cell isotropically contracts to initial strain ϵ_0^A inducing pre-tension in the network. This tension is distributed across the network using the FIRE algorithm[90] with the parameters indicated in Table S1 and maximum relaxation steps 10^7.

The additional dynamical effect is modeled in two ways. In the first case, the *active* cell isotropically contracts by 1% of R_0. In the second case, only one node of the active cell (the closest to the *passive* one) is displaced. The latter case simulates a focal adhesion site. The velocity of the nodes is set along the radial direction according to eq. 3.

The nodes of the *passive* cell are either fully constrained ("fixed") or not ("free"). In the "fixed" case, the force acting on the *passive* cell caused by *active* cell contraction is calculated. In the second "free" case, the displacement of the *passive* cell is measured.

Calculating the Range of Mechanical Influence. For analyzing the range of influence, the network was sectioned into 120 concentric rings, from the center of the *active* cell, of equal thickness of $\frac{1}{5}R_0$, that is, 20% of the cell radius. The average amplitude of force F_k^R over all fibers inside the k-th ring was calculated. Then, for the dynamic case, the maximum value of this force over time $(F_k^R)_D$ was determined.

RESULTS

We present results obtained by numerical simulations for traveling longitudinal waves along a single fiber or dispersing throughout a 2D fiber network embedded with two neighboring cells. Similar qualitative results were obtained for transverse waves (Figure S1). We then show differences in the range of influence due to either static or dynamic contraction of a single cell. Finally, we present the influence of viscous drag on the dynamic force reaching a neighboring *passive* cell.

Dynamic Wave Propagation along a Single Fiber. A single peak "half-sinus" shaped longitudinal displacement perturbation (U_x^A) is applied on a single linear elastic fiber of length L, at its "*active*" end, with an amplitude of 1% of total fiber length (L) (Figure 1a). The perturbation is applied slowly or rapidly, defined by the perturbation normalized impulse time $\tau_L^I = \frac{t_I}{t_L}$, with t_I being the impulse time and t_L the time needed for the perturbed wave to reach the end of the fiber. For example, the perturbation presented in Figure 1b reaches its peak within 1/5 of t_L and finishes within 2/5 t_L, with τ_L^I = 0.4. We denote time progression as $\tau_L = \frac{t}{t_L}$ (signal starts at "0" and perturbation reaches the *passive* end at "1" and then bounces back). From hereinafter, for clarity, we will keep all kinematic and mechanical parameters in a normalized manner.

Force wave (T_x^i) progression is depicted in a kymograph in Figure 1c, where the location along the fiber is denoted by $\frac{X}{L}$ ("0" denotes the *active* end and "1" the *passive* end). Depicted tension/compression is normalized by the maximal tension at the *active* end during a dynamic perturbation, $(F_x^A)_D$. Note that as the perturbation reaches the *passive* end, force rises relative to its emitted value and the perturbation is fully reflected and its phase flipped; the order of compression and tension waves is reversed due to a "fixed-end" boundary condition at the *passive* end, which acts as a "wall," that is, having infinite impedance. For comparison, the phase of the waves is depicted in Figure S2 also for "free-end" boundary condition.

We define the *passive-to-active* tension ratio as $\frac{R^P}{R^A}$, where $R^P = \frac{(F_x^P)_D}{(F_x^P)_S}$ is the maximal force exerted at the *passive* end during a dynamic perturbation (D) relative to static perturbation (S), and similarly, $R^A = \frac{(F_x^A)_D}{(F_x^A)_S}$ is the maximal dynamic force exerted at the *active* end relative to static perturbation. The *passive-to-active* tension, $\frac{R^P}{R^A}$, as a function of the perturbation impulse period, is depicted in Figure 1d. Note that the ratio $\frac{R^P}{R^A}$ ranges between 1 and 2. When the fiber is slowly perturbed ($\tau_L^I > 10$), the *passive-to-active* ratio is close to 1, meaning that the two ends experience practically the same maximal tension (i.e., static conditions). However, when the very same displacement perturbation is exerted rapidly, $1 < \tau_L^I < 10$, the tension ratio rises nonmonotonically up to 2 and remains constant at even faster exertions. In one-dimensional

https://doi.org/10.1021/acsbiomaterials.2c01049
ACS Biomater. Sci. Eng. 2022, 8, 5155−5170

case, factor of 2 is the physical limit following from the law of conservation of momentum for wave reflection from the *passive* end. Thus, the mechanical signal at the receiver end (*passive*) is much higher than the source if produced dynamically rather than quasi-statically, for the same displacement perturbation.

Note that by transitioning from static-to-dynamic conditions not only *passive*-to-*active* relative forces increase but also actual force magnitude increases, as expressed by R^{P}. Faster impulses at the *active* end lead to higher amplitude dynamic forces reaching the *passive* end, in comparison to a practically static loading (Figure 1e). Interestingly, in the extremely fast excitations, regime ($\tau_L^I < 5.97$) R^P decreases (going from $\tau_L^I = 0.2$ up to $\tau_L^I = 5.97$ with a nearly constant slope in log−log scale).

A few selected perturbation periods ($\tau_L^I = 2.18$, 2.63, 4.00, and 5.97) are specified in Figure 1d where the dynamic force ratio changes behavior. We then plot the normalized force $R_D = \frac{F_x}{(F_x^A)_D}$ over time for these specific time periods (Figure 1f−i). The letter D denotes here again maximal tension during a dynamic loading. The plots show both tension evolution experienced at the *active* end ("A") and *passive* end ("P") and the analytical solution at the *passive* end ("AP"). This demonstrates that the shape of the mechanical signal at the *passive* and *active* ends changes dramatically with the loading rate due to wave-interference effects (wave superposition). Analytical solutions perfectly match simulated results, thus validating the simulations.

Dynamic Force Propagation through a 2D Fiber Network Induced by an *Active* Contractile Cell toward a *Passive* Cell ("Fixed" Boundary Conditions). We next consider the case of two round cells embedded in a fiber network where one *active* cell isotropically twitches 1% of its radius and subsequently expands back to its original diameter (Figure 2a), thus perturbing the surrounding network, and the neighboring *passive* cell receives some of the signal. The dynamic twitch is exerted against a statically pre-stressed network, due to a preceding quasi-static isometric contraction (ε_0^A) of the *active* cell. The *passive* cell is not contracting; it keeps its shape and position throughout the simulation (i.e., having "fixed" boundary conditions). We also model the situation where only one node of an *active* cell twitches 1% of its radius (Figure S3), as well as for quick release of the twitch (Figure S4), and we demonstrate that results are similar to the case of entire cell contraction. This one-node perturbation reflects local tugging forces exerted by cells at specific focal adhesions against individual ECM fibers.[39] Figure 2b depicts the effect of dynamics on increasing the perturbation amplitude experienced by the *passive* cell. To keep notation concise as before, we denote the *dynamic-to-static* ratio as $R^P = \frac{(F_x^P)_D}{(F_x^P)_S}$. Twitch duration ($t_I$) is normalized by the time (t_N) it takes for a longitudinal wave to travel the shortest distance between the two neighboring cells. When slowly twitching, $\tau_N^I = \frac{t_I}{t_N} > 10$, the dynamic and static forces, experienced by the *passive* cell, are similar as indicated by a ratio $R^P \approx 1$. However, at faster twitches, $1 \lesssim \tau_N^I < 10$, the signal's amplitude increases dramatically by a few hundred percent relative to static conditions (3 to 6 times higher), and a peak in R^P is observed. The peak magnitude decreases with network pre-stress (ε_0^A), and network pre-stress has a negligible effect during extremely slow and fast twitches. As perturbations are applied faster ($\tau_N^I \lesssim \frac{3}{4}$), the force intensity that reaches the *passive* cell declines, and surprisingly, beyond $\tau_N^I \lesssim 0.1$, the force (R^P) falls even beneath one (i.e., below static conditions). Interestingly, the slope at very fast twitches is nearly constant in a logarithmic scale for all ε_0^A values.

Figure 2c shows the *passive-to-active* ratio, that is, $\frac{R^P}{R^A}$; where $R^A = \frac{(F_x^A)_D}{(F_x^A)_S}$ denotes the signal on the *active* cell and $R^P = \frac{(F_x^P)_D}{(F_x^P)_S}$ denotes the signal on the *passive* cell. Interestingly, network pre-stress does not significantly affect the depicted *passive-to-active* ratio $\frac{R^P}{R^A}$. When slowly twitching, $\tau_N^I > 10$, the *active* and *passive* cells experience practically the same dynamic increase, $\frac{R^P}{R^A} \approx 1$. At faster twitches, $1 \lesssim \tau_N^I < 10$, the force on the *passive* cell is much more prominent relative to the *active* cell, and the *passive-to-active* ratio ($\frac{R^P}{R^A}$) rises by a few tens of percent, up to 70% (at $\tau_N^I \approx 7$), and does not show the 100% increase demonstrated for a single fiber (Figure 1d). Here again, as perturbations are applied faster ($\tau_N^I < 1$), the perturbation force that reaches the *passive* cell is declined. The slope at very fast twitches is nearly constant in a logarithmic scale.

The effect of a twitch over time is traced (Figure 2d−g) using the resultant force evolution F_x (on either cell) normalized by the *maximal* force that appeared on the *active* cell, $(F_x^A)_D$ for four selected impulses τ_N^I that cover the range of the dynamic effect ($\tau_N^I = 0.27$, 1.00, 7.02, and 22.33). We observe that specifically during relatively slow twitches ($\tau_N^I \gg 1$), the evolution of forces acting on the *passive* cell follows quite closely the forces exerted by the *active* cell (Figure 2d). One can notice a slightly delayed pull on the *passive* cell, with "negative" force peaks at $\tau_N = \frac{t}{t_N} = 1.2$ normalized time units required for information to travel from the *active* cell to the *passive* cell and then a pushback ("positive" force) on the *passive* cell close to the end of *active* cell contraction. For perturbations executed very fast (Figure 2g), large and maintained force fluctuations are experienced by the *active* cell but practically negligible mechanical perturbation impinges on the *passive* cell. For the extremely rapid perturbation impulse ($\tau_N^I = 0.27$), the time evolution of fiber deformation throughout the network shows that significant fiber deformation is confined within a narrow band at close vicinity around the *active* cell (Movie S1), visually demonstrating the confinement of mechanical elastic impulse energy. For comparison, a movie for $\tau_N^I = 7.02$ is also included (Movie S2). Snapshot images from Movies S1 and S2 are described in Figure 2h,i for two extreme impulses $\tau_N^I = 7.02$ and 0.27, demonstrating the long-range spread of forces and the confinement of the mechanical signal, respectively.

In addition, we explore the effect of a wider range of network and cell configuration parameters on the propagation on the dynamic signal, and specifically, we studied the influence of (i) network connectivity (κ) (Figure S7); (ii) network density (ρ_{links}) (Figure S8); and (iii) normalized cell-to cell distance ($\frac{d}{R_0}$) (Figure S9) and level of cell contraction (Figure S10). In all cases, normalized graph showed similar trends, as demonstrated in Figure 2.

Wave Propagation in the 2D Fibrous Network Induced by an *Active* Cell toward a Compliant *Passive* Cell (Free-Boundary Conditions). Simulations up to now

https://doi.org/10.1021/acsbiomaterials.2c01049
ACS Biomater. Sci. Eng. 2022, 8, 5155−5170

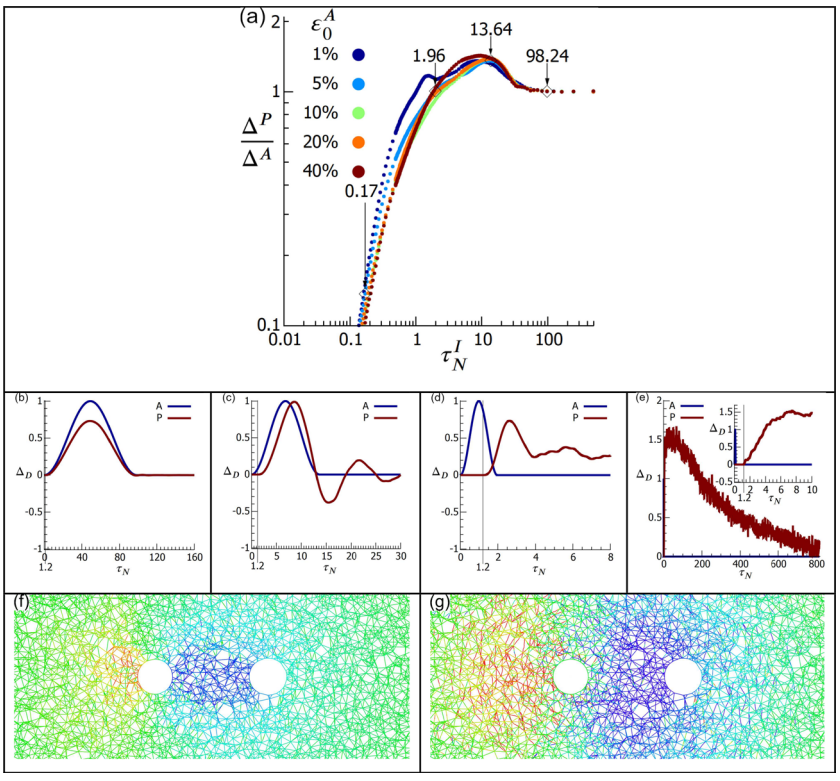

Figure 3. Dynamic signal amplification in a network with a "free-end" *passive* cell. (a) Ratio of maximum displacements of the *passive* cell nodes (considering half-sided nodes that point toward the neighboring cell) to displacement in the static case, Δ^P/Δ^A. (b−e) Displacement versus time ($\tau_N = \frac{t}{t_N}$) on the right part of the *active* cell (A) and the left part of the *passive* cell (P). The effect of a twitch over time on both cells for τ_N^I = 98.24 (b), 13.64 (c),1.96 (d), and 0.17 (e) quantified by $\Delta_D = \frac{U_x}{(U_x^A)_D}$, the displacement evolution U_x normalized by the maximal displacement that appeared on the *active* cell. The inset in panel "e" shows a shorter time interval. (f,g) Snapshot images show fiber displacement U_x at the time corresponding to the maximum displacement of the passive cell for τ_N^I = 13.64 (f) and 0.17 (g). U_x is normalized by the maximal displacement that appeared on the *active* cell. See corresponding Movie S3 for the case of τ_N^I = 0.17.

were performed on a "spatially fixed" *passive* cell (Figure 2), mimicking classical boundary conditions similar to that of a rope tied and fixed at its end (Figure 1). We were interested to explore the other extreme in "boundary conditions" where the fiber is unrestrained at its end and therefore free to displace and deform. We expect theoretically that the displacement at the *passive* end would double the displacement at the *active* end, for fast twitches, which is indeed the case for a single fiber, as demonstrated in Figure S2b. Next, we proceeded to simulate the corresponding random fiber network conditions for two neighboring cells where one cell actively twitches, as before, 1% of its radius (isotropic), thus perturbing the surrounding network, and consequently, its neighboring *passive* cell (not fixed) receives some of the signal (Movie S3). As before, the case of one cell-node contraction appears in Figure S5. The average displacement of the *passive* cell nodes under static pull by a contracted neighboring *active* cell is denoted by $(U_x^P)_S$, and the displacement of the same nodes under dynamic twitch conditions is denoted by $(U_x^P)_D$. We denote the dynamic-to-static ratio $\frac{(U_x^P)_D}{(U_x^P)_S}$ by the letters Δ^P (for the *passive* cell), and similarly, $\Delta^A = \frac{(U_x^A)_D}{(U_x^A)_S}$ (for the *active* cell). Note that Δ^A = 1, always, as we control the mechanical excitation. Figure 3a depicts the dynamic effect Δ^P on increasing the displacement amplitude as experienced by the *passive* cell. When slowly twitching, τ_N^I > 100, the dynamic and static displacements, experienced by the *passive* cell, are similar as indicated by the ratio $\Delta^P \approx 1$. At faster twitches, $1 < \tau_N^I < 100$, the signal that reaches the passive cell may increase by 40% relative to static conditions. A peak in the dynamic-to-static displacement ratio is observed around τ_N^I = 10. Note that at these compliant-cell conditions (Figure 3a), the peak appears at the same order of magnitude excitations compared to fixed-boundary conditions (Figure 2c; where the peak was in force, not displacement). Network pre-stress does not significantly affect peak amplification (either its value or dependence on impulse period). As perturbations are applied faster ($\tau_N^I \lesssim 2$), the signal amplitude that reaches the *passive* cell declines. At very fast twitches, the slope is nearly constant in log−log scale. The effect of a twitch over time (displacement evolution U_x normalized by the maximal displacement that appeared on the active cell $\Delta_D = \frac{U_x}{(U_x^A)_D}$) on both cells is shown for four impulse periods τ_N^I = 0.17, 1.96, 13.64, and 98.24 (Figure 3b−e). The displacement of the *passive* cell nodes follows quite closely the *active* cell radial displacement and relaxes back to its original size, specifically during relatively slow twitches. For perturbations executed very fast (Figure 3e), a "caged" impulse (at vicinity to the *active* cell) induces a persistent displacement of the *passive* cell that subsequently decays very slowly. Snapshot images of displacement distribution are shown for two extreme cases of τ_N^I = 0.17 (Movie S3) and 13.64 (Figure 3f,g). In summary, dynamic signal amplification is observed

https://doi.org/10.1021/acsbiomaterials.2c01049
ACS Biomater. Sci. Eng. 2022, 8, 5155−5170

also for another extreme case where the neighboring cell is compliant and free to displace and change its shape.

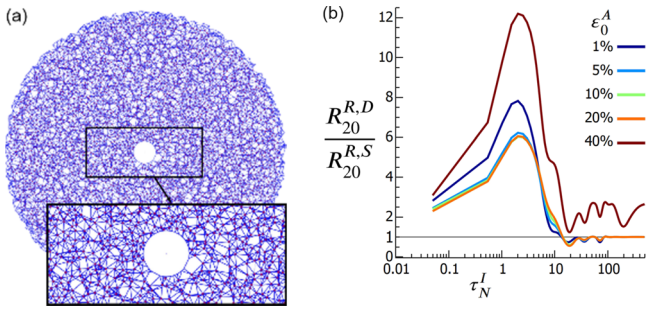

Figure 4. Dynamic versus static range of influence in the case of a single cell contracting against a 2D fibrous network. (a) Model of a single cell embedded within a 2D fibrous network. (b) Dynamic-to-static ratio of the range of influence with a 20% cutoff force decay as a function of impulse time τ^I_N. Here, for the case of a single cell, τ^I_N denotes the impulse time t_I of the single cell normalized by t_N calculated for two cells $4R_0$ apart (chosen arbitrarily for normalization).

Range of Influence Extends when Force Propagates Dynamically Rather than Statically. The propagation range of transmitted forces in the ECM is a critical parameter in determining the possible range of cell−cell mechanosensing. We thus evaluate the propagation of forces, emanating from a single cell twitch, over a 2D fibrous network (Figure 4a). Following the initial quasi-static cell contraction (network pre-stretch phase), the average magnitude of forces acting on the nodes comprising the cell perimeter was calculated, $(F^A)_S$. Then, the cell twitched 1% of its radius at different impulse periods, and the maximum value of the average force $(F^A)_D$ at the cell perimeter was calculated as a function of distance away from the cell (Methods). To evaluate the range of influence, we chose the distance at which force decays to 20% of its maximum value at the cell perimeter, referred to as $R^{R,D}_{20}$, and plotted it as a function of impulse time. We repeated the same procedure for the static case, that is, calculating the range $R^{R,S}_{20}$. The ratio of distances for the dynamic and static cases, $R^{R,D}_{20}/R^{R,S}_{20}$, corresponding to a 20% force cutoff value is shown in Figure 4b. The plot shows a peak in the influential range for an optimal impulse duration ($1 < \tau^I_N < 10$), where the range of signal propagation is amplified (about 6−12 times larger in the dynamic versus static case). Similar results were obtained when the cutoff value was chosen to be 10% of maximal force, that is, the ratio $R^{R,D}_{10}/R^{R,S}_{10}$ (Figure S6). For a cutoff of 20%, the dynamic signal spreads as much as an order of magnitude more than the static one, and in the case of 10% cutoff, this difference is equal to four times (Figure S6).

Effect of Viscosity of the ECF on Wave Propagation along ECM Fibers. To examine the effect of viscosity, we first analyzed the amplitude of a longitudinal wave excited in a linear chain (Figure 5a), similar to the one depicted in Figure 1a, with or without a viscous liquid. We used a viscosity value of 0.7 since it was reported to be the relevant magnitude of viscosity of the ECF at 37 °C.[91,92] In the viscous case, the maximal amplitude is ∼20% lower relative to the inviscid case, and the wave shape loses symmetry as its peak shifts slightly toward the *active* end (∼5% of chain length); see Figure 5a. Analytical analysis of the governing equations in the viscous and inviscid cases (see Methods) (dashed lines in Figure 5a) corroborates our mass-spring simulations. We then study the effect of viscosity on the dynamic force increase, in a linear chain, as it is dependent on impulse duration (τ^I_L) (Figure 5b,c). In the viscous case, the longitudinal wave follows closely the wave dynamics in the inviscid case down to $\tau^I_L \sim 4$. As the excitations get faster, a moderate decrease (∼30% when $\tau^I_L <$ 2) in the dynamic force ratio is demonstrated (Figure 5b). Transverse waves are a major route for elastodynamic dissipation as observed by the monotonic decrease in the dynamic force ratio as the impulse duration shortens (Figure 5c). The superposition peaks due to wave interference are completely quenched relative to the inviscid case. Together, the single-fiber simulations indicate that ECF viscosity reduces, but still may allow for dynamic perturbation propagation along embedded ECM fibers through longitudinal waves.

We turned to simulating a 2D network that is similar to that appearing in Figure 2 but this time the network is embedded in a viscous fluid. We focus on the maximal dynamic force that reaches the *passive* cell. To be able to compare different cell-to-cell distances, we normalized the force value to the dynamic force that reaches this *passive* cell when $\tau^I_N = 1$, that is, $R^P_I = {(F^P_x)_D}/{(F^P_x)_D|_{\tau^I_N=1}}$. The ratio R^P_I dramatically increases from a minimal value at the static ($\tau^I_N \to \infty$) case to a maximum at the dynamic case ($\tau^I_N \sim 1$), both in viscous and the inviscid

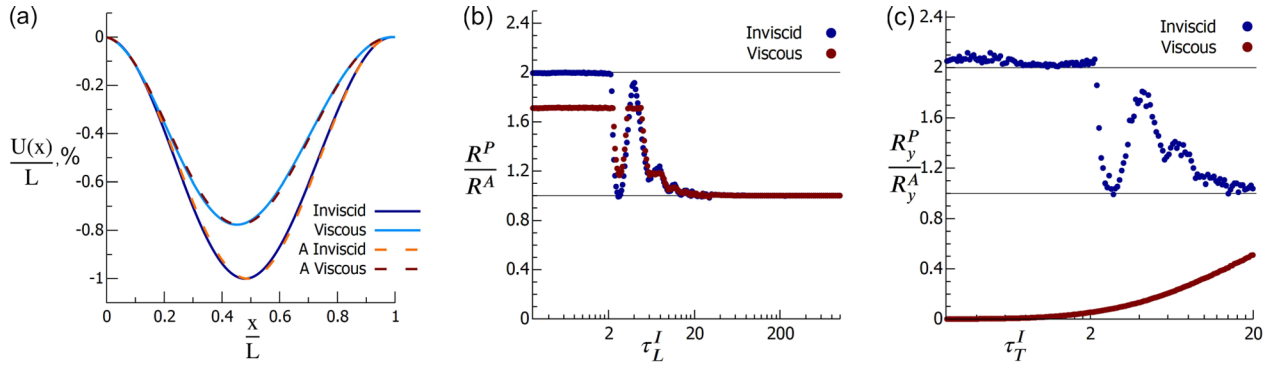

Figure 5. Effect of viscosity of the medium using single-fiber simulations. (a) Snapshot−like scheme of a longitudinal (X-displacement) wave along a linear chain of length L calculated at time t_L (at this exact time, the impulse reaches the *passive* end). The wave is a result of a pull−push perturbation at $\tau^I_L = 1$ in either viscous or inviscid environments (similar conditions to simulations presented in Figure 1). Simulation results are compared with an analytical solution (dashed lines). (b,c) Wave propagation through a chain for longitudinal (b) and transverse perturbations (c). In the transverse perturbation case (c), an initial pre-stretch was set to $\varepsilon^A_0 = 30\%$ of chain length.

https://doi.org/10.1021/acsbiomaterials.2c01049
ACS Biomater. Sci. Eng. 2022, 8, 5155−5170

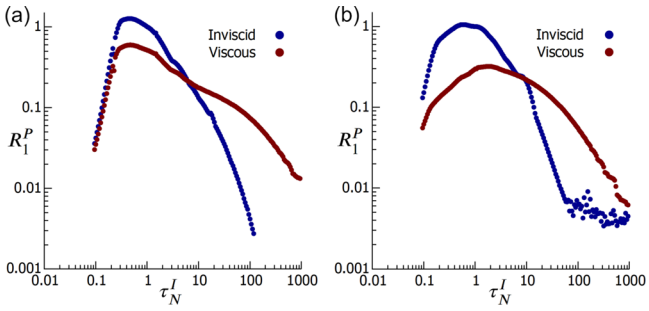

Figure 6. Effect of viscosity on wave propagation through a 2D fibrous networks (network connectivity, $\kappa = 3.6$) induced by an *active* cell toward a neighboring (two cell−cell distances considered $d = 4R_0$ and $d = 6R_0$) *passive* cell. Pre-stress is $\varepsilon_0^A = 5\%$ and the *active* cell contraction is $\varepsilon^A = 1\ \%\ R_0$. Simulations were conducted either in inviscid (blue dots) or in viscous (brown dots) environment, for two cell−cell distances: (a) $d = 4R_0$ and (b) $d = 6R_0$. The graphs shows the force acting on the *passive* cell normalized to its magnitude at time $\tau_N^I = 1$ as a function of τ_N^I.

environment (Figure 6). However, the maxima in R_1^P for networks in viscous environment are between 40% (Figure 6a, smaller cell−cell distance) to 70% (Figure 6b, larger cell−cell distance) smaller in comparison to the inviscid case. Thus, viscosity has a larger impact on the value of R_1^P when cells are farther away from each other, with viscous R_1^P about twice lower when d increases from $4R_0$ to $6R_0$. The dynamic increase in R_1^P is more pronounced in floppy (hypostatic) networks having low connectivity ($\kappa = 3.6$, Figure 6) than in rigid (hyperstatic) networks ($\kappa = 7.8$, Figure S11).

DISCUSSION

Long-range mechanical communication between cells refers to the process in which cells sense mechanical forces and tension gradients exerted by adjacent cells, where the traction stresses are mediated by deformations created in the compliant substrate. Such mode of mechanical communication has been studied for more than a decade now;[12,93,94] however, the focus has been mainly centered on relatively static or quasi-static forces.[24,95−98] In this paper, we explore the plausibility and efficacy of dynamic mechanical communication mediated by traveling wave packets along random elastic fibrous networks reflecting the ECM that surrounds living cells. Indeed, the dispersion and relaxation of elastic waves in fibrous materials has been studied,[99−104] however, not in the context of cell-to-cell communication through the ECM. Our simulations indicate that dynamic mechanical perturbations exerted by cell contractile forces may provide a potential mechanism of vibrational communication between cells. Though the literature on force propagation through the ECM fibers is vast, with abundant theoretical and numerical modeling studies, a majority of these studies have focused on static forces. The dynamic effect has not been under focused investigation probably due to the lack of experimental data of such small and rapid dynamic forces propagating in a soft gel material. It may also be related to the challenges associated with modeling elastodynamic forces in complex structures and environments, such as random fibrous networks, which are not classical engineering materials, as well as their fluid−structure interactions.[105]

In this work, we have presented numerical and analytical calculations for the propagation of both longitudinal and transverse waves along a single fiber, and we then proceeded to simulate wave propagation between cells through a network of random fibers (i.e., minimal model of the ECM). We used a particle-based model to describe fiber behavior in the network where each fiber is represented by a set of nodes with point masses moving in a flat plane due to a linear interaction between the neighboring nodes, action of the external forces, and boundary conditions. We show that for both a single fiber and a 2D fibrous network, when the *active* end (e.g., contractile cell) applies a dynamic perturbation, the *passive* end (e.g., a neighboring passive cell) receives a significantly stronger mechanical signal, for both cases of "fixed *passive* end" and "free *passive* end" boundary constrains. We also verify that the dynamic effect persists in various network configurations and cell parameters, including different network connectivities and densities, and for various degrees of cell contraction and cell−cell distances. The perturbation is considered as a dynamic one if the perturbation impulse is about 1 order of magnitude faster relative to the time needed for the wave to reach the other end (i.e., propagation period), $1 \lesssim \tau_N^I < 10$. In comparison, quasi-static perturbations are at least an order of magnitude slower, that is, $\tau_N^I > 10$. The observed dynamic amplification phenomenon may be explained physically by the effect of impinging mechanical momentum and its subsequent push-back at the boundary of the *passive* cell. We demonstrate here that the ratio of impulse duration to its propagation period from the emitter (*active* cell) to the receiver (*passive* cell) is crucial for dynamic effects to appear. This fact supports our hypothesis that dynamic mechanical cell-ECM-cell communication may produce stronger signals.

We focus in this study on longitudinal waves, their propagation speed along a bio-fiber is given, as a first approximation, by $C_L \approx \sqrt{E/\rho_{fiber}}$, where E is Young's tension modulus and ρ_{fiber} is the mass density of the fiber. The elastic modulus of a collagen-I fiber (in aqueous conditions) has been estimated to be between 30 and 80 MPa, at low tensile strains.[106−109] Similarly, a fibrin fiber has $E \approx 1 - 10$ [MPa].[110−112] Single-fiber mass density is estimated to be $1.35\left[\frac{g}{cm^3}\right]$.[113] Using the above equation to calculate the propagation speed, one gets $C_L \approx 200\left[\frac{m}{s}\right]$ for collagen fiber and $40\left[\frac{m}{s}\right]$ for a fibrin fiber. For two cells separated by 200 [μm], we calculate $\tau_N \sim 1$ [μs] for collagen and $\tau_N \sim 6$ [μs] for fibrin. Therefore, impulses in the microsecond time scale (1−10 μs) are expected to be amplified according to our simulations; such fast perturbations might be rare and of low amplitude but when they occur, they would be amplified. Another possibility is that the longitudinal wave propagates as a pressure wave in the bulk gel, and then, its velocity diminishes drastically. For example, fibrin bulk elastic modulus may be in the range of 100 to 10,000 [Pa], then τ_N would be in the range of 0.2 [ms]; so whether directly through a fiber or indirectly through the bulk network, dynamic amplification is expected to be observed in the μs-to-ms timescale. Cell dynamic movement and force generation may also create transverse waves. To a first approximation, transverse wave propagation velocity is $C_T \approx C_L \sqrt{\varepsilon}$ (see Supporting Information) where ε is the initial tensile strain; one can see that for the low strain regimen, C_T is about 1 order of magnitude smaller than C_L, and therefore, transverse waves may appear in a shifted slower band and depend on strain.

https://doi.org/10.1021/acsbiomaterials.2c01049
ACS Biomater. Sci. Eng. 2022, 8, 5155−5170

Surprisingly, we notice several peculiar behaviors of the spring-mass system that may not be initially considered straightforward. For a single fiber, for example, a non-monotonic increase in the *passive* to *active* normalized force ratio (R^P/R^A) is observed as the impulse period shortens (Figure 1d). Specifically, at medium stimulation periods ($2 < \tau_L^I < 20$), large fluctuations appear in the force ratio R^P/R^A (Figure 1d). These fluctuations are interpreted as the result of wave interference effects between waves emitted from the *active* end (propagating toward the *passive* end of the fiber) and waves reflected back (retrograding) from the fiber *passive* end. The impulse period range exhibits a succession of band gaps (impulse durations where impulse is not amplified) and pass bands (impulse durations where impulse is amplified). The analytic calculation shown in Figure 1f–i captures well the numerical simulation, thus supporting our numerical simulation results of force ratio fluctuations.

Similarly, another peculiar behavior is the bi-phasic dynamic force ratio (R^P), as the stimulation period shortens (Figure 1e); for $\tau_L^I > 20$, the ratio R^P is quite constant ($\cong 1$). As stimulation period shortens ($\tau_L^I < 10$), the force ratio R^P increases with a steep and nearly constant slope, meaning that the *passive* end experiences dramatically higher forces due to dynamic impact loading, forces that may reach up to about 1 order of magnitude higher.

Results for the cell-embedded networks also indicate peculiar dynamic behavior due to interference (Figure 2b). This plot demonstrates a maximum in the force-impulse relationship, indicating the existence of an optimal impulse duration. Whether cells can produce or be mechanosensitive to such optimal impulses should be confirmed experimentally in further studies. Additionally, elastic wave interference may confine wave-packet energy to the vicinity of an *active* cell. We have seen that at very fast mechanical excitations of the network ($\tau_N^I < 1$), the dynamic effect on the *passive* cell diminishes dramatically (R^P slope = 3) (Figure 2b), and R^P gets even below 1. In the network, extremely abrupt mechanical perturbations do not reach the neighboring *passive* cell and therefore mechanical communications via emitted elastic wave packets are excluded. Instead, the elastic energy is localized or encaged in the vicinity of the *active* cell (Movies S1 and S4). Thus, the network architecture behaves as a low-pass filter (having "acoustic" impedance) and isolates the *active* cell from its surroundings and neighboring cells. Note that the mechanical filtering is neither achieved here by a tuned mass-damper system nor is it the result of classic antiresonance[114] between coupled oscillators. At antiresonance frequencies, the oscillation amplitude can drop to almost zero due to destructive interference; however, in our case, we observe the signal attenuation in a wide range of high frequencies and not at a particular frequency as typical to the case of antiresonance. A complete understanding of this "localized elastic energy" phenomenon awaits further investigation that is beyond the scope of our current study; however, we wish to indicate the plausible relevance of a peculiar physical effect known as "Anderson localization"[115] to this result. Anderson localization is a general wave phenomenon (manifest itself for any type of wave) that relates to the transport (or its lack thereof) of waves through a disordered medium. Specifically, it describes the severe retardation or absence of propagation and spreading of waves in a disordered medium and therefore the wave distribution remains localized, especially where the wavelength is comparable to a system's characteristic length (e.g., average fiber length, average pore area, mean path length, etc.). Note that our random fiber network is a disordered medium. Localization occurs due to wave interference (both destructive and constructive) between multiple-scattering paths, and severe interferences can completely halt the waves inside the disordered medium. Indeed, originally described in quantum condensed matter systems,[115−117] recent relevance has been demonstrated for acoustic waves.[118−122] Anderson localization was reported also in studies of the vibrational modes of a disordered network of masses and springs.[123−126] According to our current understanding, Anderson localization is not restricted to electrons but is indeed general. However, the strength and dominance of this effect and its transition frequencies depend on spatial dimensionality of the system (either 1D, 2D, or 3D), the amount of disorder in the network (e.g., local anisotropy) and its length scale (e.g., ratio of the average fiber length and cell radius), type of disorder (e.g., nonuniform masses vs nonuniform springs), network architecture, network density, fiber crosslinking points (e.g., "welded" vs "pin" joints), mechanical boundary conditions, damping, and others. Therefore, further research should be followed up to investigate the relevance of this phenomenon for living cell dynamic mechanical communication through the ECM. Interestingly, cells sparsely embedded in the ECM often remodel the matrix around them and their environment transitions from initially being isotropic (i.e., random) to anisotropic (i.e., ordered) at their close vicinity, due to the cell-applied traction forces on ECM fibers.[7,127] Densified and oriented fiber network bands often form between two closely neighboring contractile cells.[7,11] In the context of dynamic perturbation localization ("Anderson localization"), it may be speculated that elastic energy transmission may be facilitated in the direction of order (aligned ECM bands) and the ECM may demonstrate insulating behavior along the direction of disorder. Thus, the formation of such ordered fibrous bands due to cellular remodeling may allow for effective communication of the dynamic mechanical signal and prevent its localization at the emitter end. We speculate that if cells cannot engage in ECM remodeling (e.g., due to immaturity, apoptosis, or pathology), elastic wave localization may serve as a mechanical noise attenuation mechanism. Then, an isolated cell would not "bother" neighboring cells if not being able to communicate coherently (produce sufficiently long wavelength signals).

A limitation of the current study is the use of linear springs in our model, whereas biopolymer fiber elasticity is rather nonlinear.[11] Even a relatively simple spring can show nonlinear phenomena including periodic, quasiperiodic, chaotic motions, hysteresis, and harmonic distortion.[128] The fibers in our simulations compress or stretch in a single transverse plane, whereas real fibers may bend (or twist) out of plane due to fiber shape and its kinematic constraints.[100] We chose to use linear springs in our model because we expect cells to exert very small displacements (low amplitude transverse and longitudinal waves). Moreover, biological fiber networks are not merely elastic, but also exhibit inherent (i.e., fiber intrinsic) visco-plastic behavior.[127,129−131] Fiber plasticity was described to influence force propagation and mechanical interaction between neighboring cells.[7,89,127,132] The model presented in this study should be extended in future studies with simulations of nonlinear fibers that may buckle and strain-stiffen as well as with viscoelastic fibers that may plastically deform at strains above the yield strain.[11,133] Notwithstanding,

https://doi.org/10.1021/acsbiomaterials.2c01049
ACS Biomater. Sci. Eng. 2022, 8, 5155−5170

plastic remodeling, due to proteolytic degradation and crosslinking sites dynamically binding and unbinding, is expected to be order of magnitudes slower than elastodynamic perturbation propagation time[127] (Malandrino et al. report a "zero-force unbinding characteristic time" on the order of tens of minutes). Indeed, plastic slow change is accumulated over time and is expected to affect dynamic signal transmission.

Viscosity of the interstitial medium is another key factor that is critical to consider that can lead to influence on wave propagation and dynamical effects. A dominant source of elasto-dynamic loss is due to the viscosity of the medium wherein fibers are immersed, typically water-like media under physiological conditions. Some of the elastic energy is transformed to heat near the fiber interface, due to the shear and transversal displacement of the surrounding fluid (ECF). Therefore, we have considered in our simulations also the case in which the fibers are embedded in a viscous liquid having a viscosity of 0.7 [mPa · s]. The choice of this viscosity value is derived from two main considerations: (i) similar values were also used in the literature for interstitial fluid at body temperature (37 °C), for example, 0.78[91] and 0.72 [mPa · s];[92] and (ii) in in vitro culture conditions, cells are typically grown in fibrous hydrogels supplemented with standard media having a low viscosity, which is close to that of pure water, 0.69 [mPa · s], at 37 °C.[134]

By introducing a viscous fluid contribution into our model, the fiber network's mechanical behavior has not only an elastic component but also a viscous component. In rheology of bulk collagen gels, a smaller difference between G' and G'' was measured at high sweep frequencies,[135,136] suggesting that at fast perturbations, the elastodynamic waves dissipate greatly. However, in our system, one should keep in mind that the mechanical signal propagates longitudinally thorough individual fibers and not homogeneously through the whole bulk. Therefore, the dominant factor in dynamic mechanical signal propagation between cells is the single-fiber interaction with the viscous fluid. We show in the single-fiber and fibrous network simulations that ECF viscosity reduces, but still allows for dynamic perturbation propagation along ECM fibers. Viscosity resulted in quenching of transverse waves but still allowing for propagation of longitudinal waves. Our current model assumes that an elastic fiber embedded in a fluid dissipates its elastodynamic energy either by shearing the liquid or by pushing against it. We did not include a plausible pathway for a relatively lossless wave propagation passing through the core of the fiber, which would require a more elaborate fiber model that supports radial modes (Poisson ratio-dependent contraction and expansion of fiber sections, an effective densification and rarefaction). The interaction of such modes with the fluid is deferred to future work.

The presented hypothesis on dynamic force amplification indicates gaps in the literature and stimulates further research questions that should be explored. For example, regarding network architecture, we have mentioned the possibility that bands of dense and oriented ECM fibers might be functional for dynamic cell−cell communication. Are they indeed waveguides for very quick (wave speeds) dissemination and sharing of information between cells? Or more generally, which dynamic cellular remodeling or physical constraints may limit or accelerate the propagation of vibrational information across the ECM? Do cells tune their mechanosensitivity to different vibration frequencies by adapting their morphology or traction forces? We have shown that ECM-embedded cells may exert static force through force chains.[5] How dominant are force chains in dynamic wave propagation? The fact that we see different dynamic responses at different impulse periods indicates that paths of force chains used by static forces is likely different in the dynamic case. However, the intensity of both static and dynamic signals is not expected to decay monotonically, not only due to local network heterogeneity but also due to reflections and wave interference. It would be illuminating to explore the differences in response to vibrational mechanical stimulation between cells embedded in oriented and strained fibrous gels (e.g., nonlinear elastic fibrin and collagen-I) relative to cells embedded in or attached on top of nonfibrous gel (linear elastic poly-acrylamide, agarose, or gelatin).

Finally, the dynamic communication hypothesis raises more questions about cell-to-cell mechanical interactions through the ECM. For example, tensed ECM fibers have natural modes of vibration, and therefore, a question arises whether there are characteristic *resonant intercellular distances* where minute cellular fluctuations build up resonantly and induce a significant effect on its neighbor cell or maybe certain frequencies emitted from an *active* cell are in resonance with the *passive* cell itself or structures within it. Interestingly, measurements of spontaneous cellular vibratory motions of osteocytes (amplitude of ∼80 nm, at 34 and 86 Hz frequency range) have recently implied that osteocytes dynamic motion is involved in cellular mechanotransduction.[137] In addition, often, spread cells are polar (i.e., exert contractions along a specified axis). Thus, it will be interesting to examine the effect of *in-plane* vibrations versus perpendicular propagating vibrations. For example, for cardiomyocytes, it has been shown that cells stimulated in the direction parallel to sarcomere alignment did not respond to an oscillatory mechanical stimulus. Only cells stimulated in the direction perpendicular to sarcomere orientation were paced.[15] The fibrous nature of the bio-hydrogel (fiber alignment and tension) contributes to dynamic synchronization between cells.

Finally, a critical aspect of communication is its spatial range. It was shown that for quasi-static cellular tractions propagating through the linear elastic substrate, the range of mechanical communication is about 50 μm and can extend to 500 μm if the substrate is nonlinearly elastic (fibrous).[13,138−140] Specifically, simulations and analytical formulations for the decay of cell-induced forces in the static case were investigated previously in depth showing the direct effect of the nonlinear properties of fibrous networks, such as fiber buckling, stiffening, and network alignment in increasing the range of force propagation.[24,95−98,141−145] In all of these cases, the static condition was considered, and force was shown to decay over distance, with the decreasing force amplitudes reaching the distant *passive* cell, relative to the force applied by the *active* cell. The range of propagation depended on the nonlinear properties of the fibrous network. Here, in contrast, we show that in the dynamic regime, forces not only decay more slowly but may also be truly amplified at the receiving *passive* cell. In comparison to static force spatial spread, where only mechanical work (force times distance) is invested by the contracting cell, we show that dynamic force propagation may spread even further because also mechanical power is delivered (force times velocity). This power creates momentum that is delivered to an extent in the viscous medium (especially through longitudinal waves). When reaching a neighboring cell, this conservation of momentum induces higher impinging

https://doi.org/10.1021/acsbiomaterials.2c01049
ACS Biomater. Sci. Eng. 2022, 8, 5155−5170

force in the bounce-back, exercising a mechanical impulse (force over time).

In our simulations of the fibrous network, we show that the dynamic mechanical signal range may be up to an order of magnitude higher than the static range signal (Figure 4b), even if for a short duration if an impulse is exerted once only. Repeated fast impulses will endure longer and their region of influences is expected to be extensive. It is clearly evident that force decay is different in the static versus dynamic case, and further research is needed to explore this observation.

CONCLUSIONS

In summary, our simulations demonstrate the impact of ECM architecture and viscosity on dynamic force propagation between contractile cells. They provide motivation for future biological experiments in mechanobiology to investigate, on the one hand, the dynamics of wave propagation in ECM environments and, on the other hand, the mechanosensitivity of cells to dynamic vibratory forces traveling and guided by the ECM. Experimental measurements of the dynamic vibroscape for cellular events, in terms of both cell-induced vibrations and cells response to vibrations, are necessary to map the relevance and importance of dynamic mechanical communication in a viscous ECF environment. ECM mechanically couples closely neighboring living cells, and dynamic mechanical communication between such cells may enable higher information content transmission, noise filtration, and faster and larger ranged signal transmission and facilitate energetically (metabolically) effective and directed transmission.

ASSOCIATED CONTENT

Supporting Information

The Supporting Information is available free of charge at https://pubs.acs.org/doi/10.1021/acsbiomaterials.2c01049.

Movie S1: Force evaluation in a network with a fixed passive cell for $\tau_N^I = 0.27$ (MP4)

Movie S2: Force evaluation in a network with a fixed passive cell for $\tau_N^I = 7.02$ (MP4)

Movie S3: Displacement evaluation in a network with a 'free' passive cell for $\tau_N^I = 0.17$ (MP4)

Movie S4: Contraction of one cell node (passive cell is 'fixed). Force evaluation in a network with a fixed passive cell for $\tau_N^I = 0.13$ (MP4)

Movie S5: Contraction of one cell node (passive cell is 'free'). Displacement evaluation for $\tau_N^I = 0.67$ (MP4)

Parameters used for the implementation of the FIRE2.0 algorithm for energy minimization in the network following *active* cell contraction; transverse perturbations in a linear chain system with a fixed end; longitudinal wave packet propagation along a single fiber, fixed, and free ends; wave propagation in the 2D fibrous network by a dynamic one cell-node displacement ("fix-boundary" conditions): dynamic perturbations in a network caused by twitching of one node on the *active* cell (*passive* cell is fixed in place); quick release from a state of pre-stretched network; wave propagation in the 2D fibrous network induced by a dynamic one-node displacement toward a compliant *passive* cell ("free-boundary" conditions); wave propagation in a 2D network induced by contraction of one cell node (*passive* cell is not fixed); range of influence with a 10% cutoff decay in force for various pre-stress (ε_0^A) values; estimation of transverse wave speed as given by longitudinal wave speed and strain; analytical solution for a wave propagation in a single fiber; dynamic force propagation through a 2D fiber network induced by an *active* contractile cell toward a *passive* cell ("fixed" boundary conditions): network connectivity, network density, cell-to-cell distance, and amplitude of cell contraction (ε^A); analysis of the effect of viscosity; the physical parameters of the fibers and the environment used in the simulations, wave propagation through a 2D fibrous networks (network connectivity $\kappa = 7.8$) induced by an *active* cell toward a neighboring *passive* cell, both viscous and inviscid conditions (PDF)

AUTHOR INFORMATION

Corresponding Authors

[§]**Igor E. Berinskii** − *School of Mechanical Engineering, Faculty of Engineering, Tel Aviv University, Tel Aviv 69978, Israel*; Email: igorbr@tauex.tau.ac.il

[§]**Ayelet Lesman** − *School of Mechanical Engineering, Faculty of Engineering and The Center for the Physics and Chemistry of Living Systems, Tel Aviv University, Tel Aviv 69978, Israel*; orcid.org/0000-0003-2511-4381; Email: ayeletlesman@tauex.tau.ac.il

Authors

Artem Y. Panchenko − *School of Mechanical Engineering, Faculty of Engineering, Tel Aviv University, Tel Aviv 69978, Israel*

Oren Tchaicheeyan − *School of Mechanical Engineering, Faculty of Engineering, Tel Aviv University, Tel Aviv 69978, Israel*

Complete contact information is available at: https://pubs.acs.org/10.1021/acsbiomaterials.2c01049

Author Contributions

[#]A.Y.P. and O.T. equally contributed to this work.

Funding

This work was partially funded by the Israel Science Foundation Grant Number 1474/16 (AL) and the Israel Science Foundation-Israeli Centers for Research Excellence Grant Number 1902/12 (AL).

Notes

The authors declare no competing financial interest.

[§]I.E.B. and A.L. jointly supervised this work.

ACKNOWLEDGMENTS

We thank Dr. Izhar Neder (Soreq Nuclear Research Center, Israel) and Prof. Yair Shokef (School of Mechanical Engineering, Faculty of Engineering, TAU, Israel) for fruitful discussions and providing a physical interpretation of few intriguing results and especially for indicating the relevance of *Anderson localization* phenomenon to our system (I.N.)

ABBREVIATION

t_I	impulse time
t_L	time of end-to-end longitudinal wave propagation in the fiber
t_T	time of end-to-end transverse wave propagation in the fiber
T_x^i	tension in a link i of the fiber

$\tau_L^I = \frac{t_I}{t_L}$	normalized impulse time for a longitudinal wave perturbation along a linear chain
$\tau_L = \frac{t}{t_L}$	normalized time in the context of a linear chain perturbed by a longitudinal wave
$\tau_T = \frac{t}{t_T}$	normalized time in the context of a linear chain perturbed by a transverse wave
t_N	the time it takes for a longitudinal wave to travel the shortest distance between two neighboring cells embedded in a random network
$\tau_N^I = \frac{t_I}{t_N}$	normalized impulse time for a perturbation between neighboring cells
$\tau_N = \frac{t}{t_N}$	normalized time in the context of a random fiber network
ε_0^A	initial strain dictated by *active* node(s) pre-stretch during the quasi-static phase
ε^A	dynamic strain dictated by *active* node(s) displacement during the dynamic phase
$(F_x^A)_D$, $(F_x^P)_D$	maximal tension at the *active* (A) and *passive* (P) ends during dynamic perturbation for longitudinal (x) wave
$(F_x^A)_S$, $(F_x^P)_S$	maximal tension at the *active* (A) and *passive* (P) ends during static loading
$R^A = \frac{(F_x^A)_D}{(F_x^A)_S}$, $R^P = \frac{(F_x^P)_D}{(F_x^P)_S}$	maximal force exerted at the *active* (A) and *passive* (P) ends during a dynamic perturbation (D) relative to static loading (S)
$R_D = \frac{F_x}{(F_x^A)_D}$	longitudinal force normalized to the maximal tension at the active end during dynamic loading
$(U_x^P)_S$, $(U_x^P)_D$	the average displacement of the *passive* cell nodes under static (S) and dynamic (D) pulls by a contracted neighboring *active* cell
$(U_x^A)_S$, $(U_x^A)_D$	the average displacement of the *active* cell nodes under static (S) and dynamic (D) pulls
$\Delta^A = \frac{(U_x^A)_D}{(U_x^A)_S}$, $\Delta^P = \frac{(U_x^P)_D}{(U_x^P)_S}$	dynamic-to-static displacement ratios at the *active* (A) and *passive* (P) cells
$\Delta_D = \frac{U_x}{(U_x^A)_D}$	longitudinal displacement evolution normalized by the maximal displacement that appears on the *active* cell
$R_{20}^{R,D}$, $R_{20}^{R,S}$	the distance at which force decays to 20% of its maximum value at the cell perimeter at dynamic (D) and static (S) loadings
$R_{10}^{R,D}$, $R_{10}^{R,S}$	the distance at which force decays to 10% of its maximum value at the cell perimeter at dynamic (D) and static (S) loadings

REFERENCES

(1) Harris, A. K.; Wild, P.; Stopak, D. Silicone-Rubber Substrata - New Wrinkle in the Study of Cell Locomotion. *Science* **1980**, *208*, 177−179.

(2) Cuerrier, C. M.; Pelling, A. E.*Cells, forces, and the microenvironment*; CRC Press, 2015.

(3) Kaunas, R.; Zemel, A.*Cell and matrix mechanics*; CRC Press, 2014.

(4) Goren, S.; Koren, Y.; Xu, X. P.; Lesman, A. Elastic Anisotropy Governs the Range of Cell-Induced Displacements. *Biophys. J.* **2020**, *118*, 1152−1164.

(5) Mann, A.; Sopher, R. S.; Goren, S.; Shelah, O.; Tchaicheeyan, O.; Lesman, A. Force chains in cell-cell mechanical communication. *J. R. Soc., Interface* **2019**, *16*, No. 20190348.

(6) Piotrowski-Daspit, A. S.; Nerger, B. A.; Wolf, A. E.; Sundaresan, S.; Nelson, C. M. Dynamics of Tissue-Induced Alignment of Fibrous Extracellular Matrix. *Biophys. J.* **2017**, *113*, 702−713.

(7) Natan, S.; Koren, Y.; Shelah, O.; Goren, S.; Lesman, A. Long-range mechanical coupling of cells in 3D fibrin gels. *Mol. Biol. Cell* **2020**, *31*, 1474−1485.

(8) Grekas, G.; Proestaki, M.; Rosakis, P.; Notbohm, J.; Makridakis, C.; Ravichandran, G. Cells exploit a phase transition to mechanically remodel the fibrous extracellular matrix. *J. R. Soc., Interface* **2021**, *18*, No. 20200823.

(9) Fan, Q. H.; Zheng, Y.; Wang, X. C.; Xie, R. P.; Ding, Y.; Wang, B. Y.; Yu, X. Y.; Lu, Y.; Liu, L. Y.; Li, Y. L.; Li, M.; Zhao, Y. J.; Jiao, Y.; Ye, F. F. Dynamically Re-Organized Collagen Fiber Bundles Transmit Mechanical Signals and Induce Strongly Correlated Cell Migration and Self-Organization. *Angew Chem Int Edit* **2021**, *60*, 11858−11867.

(10) Tang, X.; Bajaj, P.; Bashir, R.; Saif, T. A. How far cardiac cells can see each other mechanically. *Soft Matter* **2011**, *7*, 6151−6158.

(11) Sopher, R. S.; Tokash, H.; Natan, S.; Sharabi, M.; Shelah, O.; Tchaicheeyan, O.; Lesman, A. Nonlinear Elasticity of the ECM Fibers Facilitates Efficient Intercellular Communication. *Biophys. J.* **2018**, *115*, 1357−1370.

(12) Reinhart-King, C. A.; Dembo, M.; Hammer, D. A. Cell-Cell Mechanical Communication through Compliant Substrates. *Biophys. J.* **2008**, *95*, 6044−6051.

(13) Winer, J. P.; Oake, S.; Janmey, P. A. Non-Linear Elasticity of Extracellular Matrices Enables Contractile Cells to Communicate Local Position and Orientation. *PLoS One* **2009**, *4*, No. e6382.

(14) Viner, H.; Nitsan, I.; Sapir, L.; Drori, S.; Tzlil, S. Mechanical Communication Acts as a Noise Filter. *Iscience* **2019**, *14*, 58−68.

(15) Nitsan, I.; Drori, S.; Lewis, Y. E.; Cohen, S.; Tzlil, S. Mechanical communication in cardiac cell synchronized beating. *Nat. Phys.* **2016**, *12*, 472−477.

(16) Sapir, L.; Tzlil, S. Talking over the extracellular matrix: How do cells communicate mechanically? *Semin Cell Dev Biol* **2017**, *71*, 99−105.

(17) Angelini, T. E.; Hannezo, E.; Trepat, X.; Fredberg, J. J.; Weitz, D. A. Cell Migration Driven by Cooperative Substrate Deformation Patterns. *Phys. Rev. Lett.* **2010**, *104*, No. 168104.

(18) Nahum, A.; Koren, Y.; Ergaz, B.; Natan, S.; Goren, S.; Kolel, A.; Jagadeeshan, S.; Elkabets, M.; Lesman, A.; Zaritsky, A. Inference of long-range cell-cell mechanical communication from ECM remodeling fluctuations. *BioRxiv* **2022**, 2020-07.

(19) Bukoreshtliev, N. V.; Haase, K.; Pelling, A. E. Mechanical cues in cellular signalling and communication. *Cell Tissue Res.* **2013**, *352*, 77−94.

(20) Chiou, K. K.; Rocks, J. W.; Chen, C. Y.; Cho, S.; Merkus, K. E.; Rajaratnam, A.; Robison, P.; Tewari, M.; Vogel, K.; Majkut, S. F.; Prosser, B. L.; Discher, D. E.; Liu, A. J. Mechanical signaling coordinates the embryonic heartbeat. *Proc. Natl. Acad. Sci. U. S. A.* **2016**, *113*, 8939−8944.

(21) Cohen, O.; Safran, S. A. Elastic interactions synchronize beating in cardiomyocytes. *Soft Matter* **2016**, *12*, 6088−6095.

(22) Long, Y.; Niu, Y. D.; Liang, K. N.; Du, Y. N. Mechanical communication in fibrosis progression. *Trends Cell Biol* **2022**, *32*, 70−90.

(23) Liu, K. Z.; Wiendels, M.; Yuan, H. B.; Ruan, C. S.; Kouwer, P. H. J. Cell-matrix reciprocity in 3D culture models with nonlinear elasticity. *Bioact Mater* **2022**, *9*, 316−331.

https://doi.org/10.1021/acsbiomaterials.2c01049
ACS Biomater. Sci. Eng. 2022, 8, 5155−5170

(24) Ronceray, P.; Broedersz, C. P.; Lenz, M. Fiber networks amplify active stress. *Proceedings of the national academy of sciences* **2016**, *113*, 2827−2832.
(25) Floyd, C.; Levine, H.; Jarzynskie, C.; Papoiane, G. A. Understanding cytoskeletal avalanches using mechanical stability analysis. *Proc. Natl. Acad. Sci. U. S. A.* **2021**, *118*, No. e2110239118.
(26) Shi, Y.; Sivarajan, S.; Xiang, K. M.; Kostecki, G. M.; Tung, L.; Crocker, J. C.; Reich, D. H. Pervasive cytoquakes in the actomyosin cortex across cell types and substrate stiffness. *Integr. Biol.* **2021**, *13*, 246−257.
(27) Farina, A.*Soundscape ecology: principles, patterns, methods and applications*; Springer, 2013.
(28) Endler, J. A.*The emerging field of tremology*; Springer: Berlin, 2014.
(29) Kasas, S.; Ruggeri, F. S.; Benadiba, C.; Maillard, C.; Stupar, P.; Tournu, H.; Dietler, G.; Longo, G. Detecting nanoscale vibrations as signature of life. *Proc. Natl. Acad. Sci. U. S. A.* **2015**, *112*, 378−381.
(30) Hill, P. S. M.; Lakes-Harlan, R.; Mazzoni, V.; Narins, P. M.; Virant-Doberlet, M.; Wessel, A.*Biotremology: studying vibrational behavior*; Springer: Cham: 2019, DOI: 10.1007/978-3-030-22293-2.
(31) Cocroft, R. B.; Gogala, M.; Hill, P. S. M.; Wessel, A.*Studying vibrational communication*; Springer: Berlin, Heidelberg, 2014; Vol. 3.
(32) Mortimer, B. Biotremology: do physical constraints limit the propagation of vibrational information? *Animal Behaviour* **2017**, *130*, 165−174.
(33) Randall, J. A.Drummers and stompers: vibrational communication in mammals. In *The use of vibrations in communication: properties, mechanisms and function across taxa;*Transworld: Kerala, 2010, pp 99−120.
(34) Matthews, R. W.; Matthews, J. R.Mechanocommunication. In *Insect Behavior*; Springer, 2009; pp 291−339.
(35) Hill, M.; Mekdara, J.; Trimmer, B.; White, R. In *Structural vibration for robotic communication and sensing on one-dimensional structures*; 2015 IEEE/RSJ International Conference on Intelligent Robots and Systems (IROS), IEEE, 2015; pp 2160−2165.
(36) Hu, Q. D.; Morris, T. A.; Grosberg, A.; Levine, A. J.; Botvinick, E. L. Actively Driven Fluctuations in a Fibrin Network. *Front Phys-Lausanne* **2021**, *8*, No. 568736.
(37) Rapp, P. E. Why Are So Many Biological-Systems Periodic. *Prog Neurobiol* **1987**, *29*, 261−273.
(38) Ronceray, P.; Broedersz, C. P.; Lenz, M. Fiber plucking by molecular motors yields large emergent contractility in stiff biopolymer networks. *Soft Matter* **2019**, *15*, 1481−1487.
(39) Plotnikov, S. V.; Pasapera, A. M.; Sabass, B.; Waterman, C. M. Force Fluctuations within Focal Adhesions Mediate ECM-Rigidity Sensing to Guide Directed Cell Migration. *Cell* **2012**, *151*, 1513−1527.
(40) Doyle, A. D.; Sykora, D. J.; Pacheco, G. G.; Kutys, M. L.; Yamada, K. M. 3D mesenchymal cell migration is driven by anterior cellular contraction that generates an extracellular matrix prestrain. *Dev. Cell* **2021**, *56*, 826−841.e4.
(41) Yang, Y.; Wu, M. Rhythmicity and waves in the cortex of single cells. *Philos. Trans. R. Soc., B* **2018**, *373*, No. 20170116.
(42) Rome, L. C.; Lindstedt, S. L. The quest for speed: Muscles built for high-frequency contractions. *News Physiol Sci* **1998**, *13*, 261−268.
(43) Ijaz, F.; Ikegami, K. Live cell imaging of dynamic behaviors of motile cilia and primary cilium. *Microscopy-Jpn* **2019**, *68*, 99−110.
(44) Shlomovitz, R.; Gov, N. S. Exciting cytoskeleton-membrane waves. *Phys. Rev. E: Stat., Nonlinear, Soft Matter Phys.* **2008**, *78*, No. 041911.
(45) Krol, A. Y.; Grinfeldt, M. G.; Levin, S. V.; Smilgavichus, A. D. Local Mechanical Oscillations of the Cell-Surface within the Range 0.2-30 Hz. *Eur. Biophys. J.* **1990**, *19*, 93−99.
(46) Pelling, A. E.; Sehati, S.; Gralla, E. B.; Valentine, J. S.; Gimzewski, J. K. Local nanomechanical motion of the cell wall of Saccharomyces cerevisiae. *Science* **2004**, *305*, 1147−1150.
(47) Nikukar, H.; Reid, S.; Tsimbouri, P. M.; Riehle, M. O.; Curtis, A. S. G.; Dalby, M. J. Osteogenesis of Mesenchymal Stem Cells by Nanoscale Mechanotransduction. *ACS Nano* **2013**, *7*, 2758−2767.
(48) Tan, S. J.; Chang, A. C.; Miller, C. M.; Anderson, S. M.; Prahl, L. S.; Odde, D. J.; Dunn, A. R. Regulation and dynamics of force transmission at individual cell-matrix adhesion bonds. *Sci. Adv.* **2020**, *6*, No. eaax0317.
(49) Mishra, Y. G.; Manavathi, B. Focal adhesion dynamics in cellular function and disease. *Cell Signal* **2021**, *85*, No. 110046.
(50) Andreu, I.; Falcones, B.; Hurst, S.; Chahare, N.; Quiroga, X.; Le Roux, A. L.; Kechagia, Z.; Beedle, A. E. M.; Elosegui-Artola, A.; Trepat, X.; Farre, R.; Betz, T.; Almendros, I.; Roca-Cusachs, P. The force loading rate drives cell mechanosensing through both reinforcement and cytoskeletal softening. *Nat. Commun.* **2021**, *12*, 4229.
(51) Ingber, D. E. Tensegrity: The architectural basis of cellular mechanotransduction. *Annu. Rev. Physiol.* **1997**, *59*, 575−599.
(52) Ingber, D. E. Cellular mechanotransduction: putting all the pieces together again. *Faseb J* **2006**, *20*, 811−827.
(53) Liu, S. B.; Yang, H. Q.; Wang, M.; Tian, J.; Hong, Y.; Li, Y.; Genin, G. M.; Lu, T. J.; Xu, F. Torsional and translational vibrations of a eukaryotic nucleus, and the prospect of vibrational mechanotransduction and therapy. *J. Mech. Phys. Solids* **2021**, *155*, No. 104572.
(54) Jansen, K. A.; Donato, D. M.; Balcioglu, H. E.; Schmidt, T.; Danen, E. H. J.; Koenderink, G. H. A guide to mechanobiology: Where biology and physics meet. *Biochim. Biophys. Acta, Mol. Cell Res.* **2015**, *1853*, 3043−3052.
(55) Kim, D.; Kwon, S. Vibrational stress affects extracellular signal-regulated kinases activation and cytoskeleton structure in human keratinocytes. *PLoS One* **2020**, *15*, No. 0231174.
(56) Nekouzadeh, A.; Genin, G. M.; Bayly, P. V.; Elson, E. L. Wave motion in relaxation-testing of nonlinear elastic media. *Proc. R. Soc. A* **2005**, *461*, 1599−1626.
(57) Tijore, A.; Yao, M. X.; Wang, Y. H.; Hariharan, A.; Nematbakhsh, Y.; Doss, B. L.; Lim, C. T.; Sheetz, M. P. Selective killing of transformed cells by mechanical stretch. *Biomaterials* **2021**, *275*, No. 120866.
(58) Palumbo, S.; Carotenuto, A. R.; Cutolo, A.; Deseri, L.; Pugno, N.; Fraldi, M. Mechanotropism of single cells adhering to elastic substrates subject to exogenous forces. *J. Mech. Phys. Solids* **2021**, *153*, No. 104475.
(59) Liao, H. M.; Munoz-Pinto, D.; Qu, X.; Hu, Y. P.; Grunlan, M. A.; Hahn, M. S. Influence of hydrogel mechanical properties and mesh size on vocal fold fibroblast extracellular matrix production and phenotype. *Acta Biomater.* **2008**, *4*, 1161−1171.
(60) Kutty, J. K.; Webb, K. Vibration stimulates vocal mucosa-like matrix expression by hydrogel-encapsulated fibroblasts. *J. Tissue Eng. Regener. Med.* **2010**, *4*, 62−72.
(61) Bacabac, R. G.; Smit, T. H.; Van Loon, J. J. W. A.; Doulabi, B. Z.; Helder, M.; Klein-Nulend, J. Bone cell responses to high-frequency vibration stress: does the nucleus oscillate within the cytoplasm? *FASEB J.* **2006**, *20*, 858−864.
(62) Ozcivici, E.; Luu, Y. K.; Adler, B.; Qin, Y. X.; Rubin, J.; Judex, S.; Rubin, C. T. Mechanical signals as anabolic agents in bone. *Nat. Rev. Rheumatol.* **2010**, *6*, 50−59.
(63) Shikata, T.; Morishita, S.; Shiraishi, T.; Takeuchi, R. Effects of Acceleration Amplitude and Frequency of Mechanical Vibration on Cultured Osteoblasts. *Proc. ASME Int. Mech. Eng. Congr. Expo.* **2009**, *2*, 625−633.
(64) Tong, Z. X.; Duncan, R. L.; Jia, X. Q. Modulating the Behaviors of Mesenchymal Stem Cells Via the Combination of High-Frequency Vibratory Stimulations and Fibrous Scaffolds. *Tissue Eng. Pt A* **2013**, *19*, 1862−1878.
(65) Caberlotto, E.; Bernal, M.; Miller, Z.; Poole, A.; Ruiz, L.; Tanter, M.; Gennisson, J. L.; Querleux, B. Controlled mechanical vibration and impacts on skin biology. *Skin Res. Technol.* **2019**, *25*, 881−889.
(66) Robertson, S. N.; Campsie, P.; Childs, P. G.; Madsen, F.; Donnelly, H.; Henriquez, F. L.; Mackay, W. G.; Salmeron-Sanchez, M.; Tsimbouri, M. P.; Williams, C.; Dalby, M. J.; Reid, S. Control of cell behaviour through nanovibrational stimulation: nanokicking. *Philos. Trans. R. Soc., A* **2018**, *376*, No. 0290.

(67) Brugger, M. S.; Baumgartner, K.; Mauritz, S. C. F.; Gerlach, S. C.; Roder, F.; Schlosser, C.; Fluhrer, R.; Wixforth, A.; Westerhausen, C. Vibration enhanced cell growth induced by surface acoustic waves as in vitro wound-healing model. *Proc. Natl. Acad. Sci. U. S. A.* **2020**, *117*, 31603−31613.
(68) Noriega, S.; Mamedov, T.; Turner, J. A.; Subramanian, A. Intermittent applications of continuous ultrasound on the viability, proliferation, morphology, and matrix production of chondrocytes in 3D matrices. *Tissue Eng.* **2007**, *13*, 611−618.
(69) Imashiro, C.; Kang, B.; Lee, Y.; Hwang, Y. H.; Im, S.; Kim, D. E.; Takemura, K.; Lee, H. Propagating acoustic waves on a culture substrate regulate the directional collective cell migration. *Microsyst. Nanoeng.* **2021**, *7*, 90.
(70) Gjorevski, N.; Piotrowski, A. S.; Varner, V. D.; Nelson, C. M. Dynamic tensile forces drive collective cell migration through three-dimensional extracellular matrices. *Sci. Rep.* **2015**, *5*, 11458.
(71) Buchmann, B.; Engelbrecht, L. K.; Fernandez, P.; Hutterer, F. P.; Raich, M. K.; Scheel, C. H.; Bausch, A. R. Mechanical plasticity of collagen directs branch elongation in human mammary gland organoids. *Nat. Commun.* **2021**, *12*, 2759.
(72) Yuval, J.; Safran, S. A. Dynamics of elastic interactions in soft and biological matter. *Phys. Rev. E: Stat., Nonlinear, Soft Matter Phys.* **2013**, *87*, No. 042703.
(73) Ozkale, B.; Sakar, M. S.; Mooney, D. J. Active biomaterials for mechanobiology. *Biomaterials* **2021**, *267*, No. 120497.
(74) Tang, S. C.; Richardson, B. M.; Anseth, K. S. Dynamic covalent hydrogels as biomaterials to mimic the viscoelasticity of soft tissues. *Prog. Mater. Sci.* **2021**, *120*, No. 100738.
(75) Tran, K. A.; Kraus, E.; Clark, A. T.; Bennett, A.; Pogoda, K.; Cheng, X. M.; Cebers, A.; Janmey, P. A.; Galie, P. A. Dynamic Tuning of Viscoelastic Hydrogels with Carbonyl Iron Microparticles Reveals the Rapid Response of Cells to Three-Dimensional Substrate Mechanics. *ACS Appl. Mater. Interfaces* **2021**, *13*, 20947−20959.
(76) De Martino, S.; Netti, P. A. Dynamic azopolymeric interfaces for photoactive cell instruction. *Biophys. Rev.* **2020**, *1*, No. 011302.
(77) Vernerey, F. J.; Sridhar, S. L.; Muralidharan, A.; Bryant, S. J. Mechanics of 3D Cell-Hydrogel Interactions: Experiments, Models, and Mechanisms. *Chem. Rev.* **2021**, *121*, 11085−11148.
(78) Feliciano, A. J.; van Blitterswijk, C.; Moroni, L.; Baker, M. B. Realizing tissue integration with supramolecular hydrogels. *Acta Biomater.* **2021**, *124*, 1−14.
(79) Ma, Y. F.; Han, T.; Yang, Q. X.; Wang, J.; Feng, B. C.; Jia, Y. B.; Wei, Z.; Xu, F. Viscoelastic Cell Microenvironment: Hydrogel-Based Strategy for Recapitulating Dynamic ECM Mechanics. *Adv. Funct. Mater.* **2021**, *31*, No. 2100848.
(80) Charrier, E. E.; Pogoda, K.; Li, R. B.; Park, C. Y.; Fredberg, J. J.; Janmey, P. A. A novel method to make viscoelastic polyacrylamide gels for cell culture and traction force microscopy. *APL Bioeng.* **2020**, *4*, No. 036104.
(81) Chaudhuri, O.; Cooper-White, J.; Janmey, P. A.; Mooney, D. J.; Shenoy, V. B. Effects of extracellular matrix viscoelasticity on cellular behaviour. *Nature* **2020**, *584*, 535−546.
(82) Chandorkar, Y.; Nava, A. C.; Schweizerhof, S.; Van Dongen, M.; Haraszti, T.; Kohler, J.; Zhang, H.; Windoffer, R.; Mourran, A.; Moller, M.; De Laporte, L. Cellular responses to beating hydrogels to investigate mechanotransduction. *Nat. Commun.* **2019**, *10*, 4027.
(83) Allen, M. P.; Tildesley, D. J.*Computer simulation of liquids*; Oxford university Press, 2017.
(84) Shapovalov, V. Motion of a flexible finite-length filament in a flow of a viscous fluid. *J. Appl. Mech. Tech. Phys.* **2000**, *41*, 337−346.
(85) Vingelmann, P.; Fitzek, F. H. P.; CUDA. https://developer.nvidia.com/cuda-toolkit.
(86) Lindstrom, S. B.; Kulachenko, A.; Jawerth, L. M.; Vader, D. A. Finite-strain, finite-size mechanics of rigidly cross-linked biopolymer networks (vol 9, pg 7302, 2013). *Soft Matter* **2013**, *9*, 11712−11712.
(87) Hatami-Marbini, H.; Rohanifar, M. Mechanical response of composite fiber networks subjected to local contractile deformation. *Int. J. Solids Struct.* **2021**, *228*, No. 111045.
(88) Jansen, K. A.; Bacabac, R. G.; Piechocka, I. K.; Koenderink, G. H. Cells actively stiffen fibrin networks by generating contractile stress. *Biophys. J.* **2013**, *105*, 2240−2251.
(89) Kim, J.; Feng, J.; Jones, C. A.; Mao, X.; Sander, L. M.; Levine, H.; Sun, B. Stress-induced plasticity of dynamic collagen networks. *Nat. Commun.* **2017**, *8*, 842.
(90) Guenole, J.; Nohring, W. G.; Vaid, A.; Houlle, F.; Xie, Z. C.; Prakash, A.; Bitzek, E. Assessment and optimization of the fast inertial relaxation engine (FIRE) for energy minimization in atomistic simulations and its implementation in LAMMPS. *Comput. Mater. Sci.* **2020**, *175*, No. 109584.
(91) Teo, C. S.; Tan, W. H. K.; Lee, T.; Wang, C.-H. Transient interstitial fluid flow in brain tumors: Effect on drug delivery. *Chem. Eng. Sci.* **2005**, *60*, 4803−4821.
(92) Tien, J.; Dance, Y. W.; Ghani, U.; Seibel, A. J.; Nelson, C. M. Interstitial hypertension suppresses escape of human breast tumor cells via convection of interstitial fluid. *Cell. Mol. Bioeng.* **2021**, *14*, 147−159.
(93) Georges, P. C.; Janmey, P. A. Cell type-specific response to growth on soft materials. *J. Appl. Physiol.* **2005**, *98*, 1547−1553.
(94) Alisafaei, F.; Chen, X. Y.; Leahy, T.; Janmey, P. A.; Shenoy, V. B. Long-range mechanical signaling in biological systems (vol 63, pg 113, 2020). *Soft Matter* **2021**, *17*, 410−410.
(95) Song, D.; Shivers, J. L.; MacKintosh, F. C.; Patteson, A. E.; Janmey, P. A. Cell-induced confinement effects in soft tissue mechanics. *J. Appl. Phys.* **2021**, *129*, 140901.
(96) Sirote, C.; Shokef, Y. Mean-field interactions between living cells in linear and nonlinear elastic matrices. *Phys. Rev. E* **2021**, *104*, No. 024411.
(97) Ronceray, P.; Broedersz, C. P.; Lenz, M. Stress-dependent amplification of active forces in nonlinear elastic media. *Soft Matter* **2019**, *15*, 331−338.
(98) Golkov, R.; Shokef, Y. Elastic interactions between anisotropically contracting circular cells. *Phys Rev E* **2019**, *99*, No. 032418.
(99) Babaee, S.; Shahsavari, A. S.; Wang, P.; Picu, R. C.; Bertoldi, K. Wave propagation in cross-linked random fiber networks. *Appl. Phys. Lett.* **2015**, *107*, 211904.
(100) Reda, H.; Berkache, K.; Ganghoffer, J. F.; Lakiss, H. Dynamical properties of random fibrous networks based on generalized continuum mechanics. *Waves Random Complex Media* **2020**, *30*, 27−53.
(101) Jafari, H.; Yazdi, M. R. H.; Fakhrabadi, M. M. S. Wave propagation in microtubule-based bio-nano-architected networks: A lesson from nature. *Int. J. Mech. Sci.* **2019**, *164*, No. 105175.
(102) Gnesotto, F. S.; Remlein, B. M.; Broedersz, C. P. Nonequilibrium dynamics of isostatic spring networks. *Phys. Rev. E* **2019**, *100*, No. 013002.
(103) Dhume, R. Y.; Barocas, V. H. Emergent structure-dependent relaxation spectra in viscoelastic fiber networks in extension. *Acta Biomater.* **2019**, *87*, 245−255.
(104) Amjad, S.; Picu, R. Stress relaxation in network materials: the contribution of the network. *Soft Matter* **2022**, *18*, 446−454.
(105) Duprat, C.; Shore, H. A.*Fluid-structure interactions in low-Reynolds-number flows*; Royal Society of Chemistry, 2015.
(106) van der Rijt, J. A. J.; van der Werf, K. O.; Bennink, M. L.; Dijkstra, P. J.; Feijen, J. Micromechanical testing of individual collagen fibrils. *Macromol. Biosci.* **2006**, *6*, 697−702.
(107) Miyazaki, H.; Hayashi, K. Tensile Tests of Collagen Fibers Obtained from the Rabbit Patellar Tendon. *Biomed. Microdevices* **1999**, *2*, 151−157.
(108) Graham, J. S.; Vomund, A. N.; Phillips, C. L.; Grandbois, M. Structural changes in human type I collagen fibrils investigated by force spectroscopy. *Exp. Cell Res.* **2004**, *299*, 335−342.
(109) Stein, A. M.; Vader, D. A.; Weitz, D. A.; Sander, L. M. The Micromechanics of Three-Dimensional Collagen-I Gels. *Complexity* **2011**, *16*, 22−28.
(110) Li, W.; Sigley, J.; Pieters, M.; Helms, C. C.; Nagaswami, C.; Weisel, J. W.; Guthold, M. Fibrin Fiber Stiffness Is Strongly Affected

by Fiber Diameter, but Not by Fibrinogen Glycation. *Biophys. J.* **2016**, *110*, 1400−1410.
(111) Hudson, N. E.; Ding, F.; Bucay, I.; O'Brien, E. T.; Gorkun, O. V.; Superfine, R.; Lord, S. T.; Dokholyan, N. V.; Falvo, M. R. Submillisecond Elastic Recoil Reveals Molecular Origins of Fibrin Fiber Mechanics. *Biophys. J.* **2013**, *104*, 2671−2680.
(112) Collet, J. P.; Shuman, H.; Ledger, R. E.; Lee, S. T.; Weisel, J. W. The elasticity of an individual fibrin fiber in a clot. *Proc. Natl. Acad. Sci. U. S. A.* **2005**, *102*, 9133−9137.
(113) Morin, C.; Hellmich, C.; Henits, P. Fibrillar structure and elasticity of hydrating collagen: A quantitative multiscale approach. *J. Theor. Biol.* **2013**, *317*, 384−393.
(114) Shanmuganathan, R.; Sanjuan, M. A. F.*Nonlinear Resonances*; Springer International Publishing: Switzerland, 2016.
(115) Anderson, P. W. Absence of diffusion in certain random lattices. *Phys. Rev.* **1958**, *109*, 1492.
(116) Maynard, J. D. Colloquium: Acoustical analogs of condensed-matter problems. *Rev. Mod. Phys.* **2001**, *73*, 401−417.
(117) Lagendijk, A.; van Tiggelen, B.; Wiersma, D. S. Fifty years of Anderson localization. *Phys. Today* **2009**, *62*, 24−29.
(118) He, S.; Maynard, J. D. Detailed Measurements of Inelastic-Scattering in Anderson Localization. *Phys. Rev. Lett.* **1986**, *57*, 3171−3174.
(119) Hu, H. F.; Strybulevych, A.; Page, J. H.; Skipetrov, S. E.; Van Tiggelen, B. A. Localization of ultrasound in a three-dimensional elastic network. *Nat. Phys.* **2008**, *4*, 945−948.
(120) Dhillon, J.; Bozhko, A.; Walker, E.; Neogi, A.; Krokhin, A. Localization of ultrasound in 2D phononic crystal with randomly oriented asymmetric scatterers. *J. Appl. Phys.* **2021**, *129*, 134701.
(121) Weaver, R. L. Anderson Localization of Ultrasound. *Wave Motion* **1990**, *12*, 129−142.
(122) Ángel, J. C.; Guzmán, J. C. T.; de Anda, A. D. Anderson localization of flexural waves in disordered elastic beams. *Sci. Rep.* **2019**, *9*, 3572.
(123) Amir, A.; Krich, J. J.; Vitelli, V.; Oreg, Y.; Imry, Y. Emergent Percolation Length and Localization in Random Elastic Networks. *Phys. Rev. X* **2013**, *3*, No. 021017.
(124) Monthus, C.; Garel, T. Random elastic networks: a strong disorder renormalization approach. *J. Phys. A: Math. Theor.* **2011**, *44*, No. 085001.
(125) Beltukov, Y. M.; Skipetrov, S. E. Finite-time scaling at the Anderson transition for vibrations in solids. *Phys. Rev. B* **2017**, *96*, No. 174209.
(126) Skipetrov, S. E.; Beltukov, Y. M. Anderson transition for elastic waves in three dimensions. *Phys. Rev. B* **2018**, *98*, No. 064206.
(127) Malandrino, A.; Trepat, X.; Kamm, R. D.; Mak, M. Dynamic filopodial forces induce accumulation, damage, and plastic remodeling of 3D extracellular matrices. *PLoS Comput. Biol.* **2019**, *15*, No. e1006684.
(128) Tufillaro, N. B. Nonlinear and Chaotic String Vibrations. *Am. J. Phys.* **1989**, *57*, 408−414.
(129) Sirenko, Y. M.; Stroscio, M. A.; Kim, K. Dynamics of cytoskeletal filaments. *Phys. Rev. E* **1996**, *54*, 1816.
(130) Kučera, O.; Havelka, D.; Cifra, M. Vibrations of microtubules: Physics that has not met biology yet. *Wave Motion* **2017**, *72*, 13−22.
(131) Younesian, D.; Hosseinkhani, A.; Askari, H.; Esmailzadeh, E. Elastic and viscoelastic foundations: a review on linear and nonlinear vibration modeling and applications. *Nonlinear Dyn.* **2019**, *97*, 853−895.
(132) Ban, E.; Franklin, J. M.; Nam, S.; Smith, L. R.; Wang, H.; Wells, R. G.; Chaudhuri, O.; Liphardt, J. T.; Shenoy, V. B. Mechanisms of plastic deformation in collagen networks induced by cellular forces. *Biophys. J.* **2018**, *114*, 450−461.
(133) Orlova, D.; Panchenko, A. Y.; Omairey, S.; Berinskii, I. Computational homogenization of bio-inspired metamaterial with a random fiber network microstructure. *Mech. Res. Commun.* **2022**, *124*, No. 103930.
(134) Poon, C. Measuring the density and viscosity of culture media for optimized computational fluid dynamics analysis of in vitro devices. *J. Mech. Behav. Biomed. Mater.* **2022**, *126*, No. 105024.
(135) Sauer, F.; Oswald, L.; de Schellenberger, A. A.; Tzschätzsch, H.; Schrank, F.; Fischer, T.; Braun, J.; Mierke, C. T.; Valiullin, R.; Sack, I. Collagen networks determine viscoelastic properties of connective tissues yet do not hinder diffusion of the aqueous solvent. *Soft Matter* **2019**, *15*, 3055−3064.
(136) Zuidema, J. M.; Rivet, C. J.; Gilbert, R. J.; Morrison, F. A. A protocol for rheological characterization of hydrogels for tissue engineering strategies. *J. Biomed. Mater. Res., Part B* **2014**, *102*, 1063−1073.
(137) Wu, X. T.; Xiao, W.; Cao, R. Y.; Yang, X.; Pan, F.; Sun, L. W.; Fan, Y. B. Spontaneous cellular vibratory motions of osteocytes are regulated by ATP and spectrin network. *Bone* **2019**, *128*, 112056.
(138) Korff, T.; Augustin, H. G. Tensional forces in fibrillar extracellular matrices control directional capillary sprouting. *J. Cell Sci.* **1999**, *112*, 3249−3258.
(139) Stopak, D.; Harris, A. K. Connective-Tissue Morphogenesis by Fibroblast Traction. 1. Tissue-Culture Observations. *Dev. Biol.* **1982**, *90*, 383−398.
(140) Ouyang, M. X.; Qian, Z. L.; Bu, B.; Jin, Y.; Wang, J. J.; Zhu, Y. M.; Liu, L.; Pan, Y.; Deng, L. H. Sensing Traction Force on the Matrix Induces Cell-Cell Distant Mechanical Communications for Self-Assembly. *ACS Biomater. Sci. Eng.* **2020**, *6*, 5833−5848.
(141) Ruiz-Franco, J.; van Der Gucht, J. Force Transmission in Disordered Fibre Networks. *Frontiers in Cell and Developmental Biology* **2022**, *10*, No. 931776.
(142) Broedersz, C. P.; Mao, X.; Lubensky, T. C.; MacKintosh, F. C. Criticality and isostaticity in fibre networks. *Nat. Phys.* **2011**, *7*, 983−988.
(143) Ronceray, P.; Lenz, M. Connecting local active forces to macroscopic stress in elastic media. *Soft Matter* **2015**, *11*, 1597−1605.
(144) Wang, H.; Xu, X. Continuum elastic models for force transmission in biopolymer gels. *Soft Matter* **2020**, *16*, 10781−10808.
(145) Chen, X.; Chen, D.; Ban, E.; Toussaint, K. C.; Janmey, P. A.; Wells, R. G.; Shenoy, V. B. Glycosaminoglycans modulate long-range mechanical communication between cells in collagen networks. *Proceedings of the National Academy of Sciences* **2022**, *119*, No. e2116718119.

https://doi.org/10.1021/acsbiomaterials.2c01049
ACS Biomater. Sci. Eng. 2022, 8, 5155−5170